Transp Porous Med (2009) 80:401–430
DOI 10.1007/s11242-009-9369-2

Upscaling Non-Darcy Flow

C. R. Garibotti · M. Peszyńska

Received: 27 April 2008 / Accepted: 18 February 2009 / Published online: 13 March 2009

Abstract We consider upscaling of non-Darcy flow in heterogeneous porous media. Our approach extends the pressure-based numerical homogenization procedure for linear Darcy flow, due to Durlofsky, to the nonlinear case. The effective coefficients are not constants but rather mildly varying functions of prevailing gradients of pressure. The upscaled model approximates the fine grid model accurately and, in some cases, more accurately than what is expected for Darcy flow; this is due to the non-Darcy effects which suppress heterogeneity. We provide comparisons of alternative approaches as well as consider several variants of numerical realizations of the non-Darcy flow model. Numerical results show effectiveness of the upscaling procedure.

Keywords Non-Darcy flow · Upscaling · Numerical homogenization · Finite differences · Mixed finite elements

1 Introduction

When modeling flow and transport in heterogeneous porous media using numerical methods, one often needs to consider a scale H coarser than the h scale at which the data are given. Over the last two or three decades, various techniques of *upscaling* from scale h to H, also called *numerical homogenization*, have been defined and critically evaluated [see original articles (Durlofsky 1991), review (Renarda and de Marsily 1997), and recent work (Zijl and Trykozko 2002; Holden and Nielsen 2000; Chen et al. 2003; Chen and Durlofsky 2006)]. While methods of upscaling for linear single equation models are reasonably well understood, upscaling nonlinear models or systems, beyond the progress made for multiphase flow

C. R. Garibotti · M. Peszyńska (✉)
Mathematics Department, Oregon State University, Corvallis, OR 97331, USA
e-mail: mpesz@math.oregonstate.edu

C. R. Garibotti
e-mail: crgaribotti@sinmec.ufsc.br

(Durlofsky 2002; Efendiev et al. 2006; Chen and Durlofsky 2006), remains, in general, an open field.

In this article, we are concerned with upscaling of non-Darcy model of single-phase incompressible fluid flow in saturated porous medium $\Omega \subset \mathbb{R}^d$, $d = 1, 2, 3$, in the form

$$(\mathbf{K}^{-1} + \beta \mathbf{I}|\mathbf{u}|)\mathbf{u} = -\nabla p. \tag{1}$$

This extends the linear Darcy's law

$$\mathbf{u} = -\mathbf{K}\nabla p, \tag{2}$$

with p denoting pressure or potential, $\mathbf{K}$ denoting the hydraulic conductivity tensor, $\mathbf{I} \in \mathbb{R}^{d\times d}$ the identity matrix, and where $\mathbf{u}$ is the velocity (volumetric flux) of the fluid. Here, β is the nonnegative scalar known as the Forchheimer coefficient, and the model (1) is due to Forchheimer (1901). Clearly, if $\beta = 0$, then (1) reduces to (2). Other formulations are available in literature; we develop these and the notation in Sect. 2.

The conservation of mass is given by

$$\nabla \cdot \mathbf{u} = 0, \tag{3}$$

or, more generally, with a distributed source q by

$$\nabla \cdot \mathbf{u} = q. \tag{4}$$

The central issue addressed in this article concerns heterogeneous porous media when $\mathbf{K} = \mathbf{K}(\mathbf{x})$, $\mathbf{x} \in \Omega$. We assume $\beta \equiv$ const or $\beta = \beta(\mathbf{x})$ which occurs for example when β is correlated to $\mathbf{K}$ via some relationship $\beta = g(K)$.

Specifically, the natural question that arises is how to *upscale* the model (1) and (3). That is, given values of $\mathbf{K}_h$ and β_h at a scale h, what values of $\mathbf{K}_H$ and β_H should one use in a numerical model at a scale $H \gg h$? In particular, if β_h is constant, is it appropriate to assume so for β_H? Similar questions arise when β_h is not constant but rather correlated to $\mathbf{K}_h$; the answers are not straightforward due to nonlinearity of (1).

For the linear case, i.e., Darcy's flow (2) and (3), various *upscaling* and numerical homogenization methods have been shown to be very effective (see Durlofsky 1991; Renarda and de Marsily 1997; Chen et al. 2003; Holden and Nielsen 2000). Combine (2) and (3) and consider a numerical approximation on grid parametrized by h of the resulting elliptic PDE, $-\nabla_h \cdot (\mathbf{K}_h \nabla_h p_h) = 0$. Upscaling to scale H means we want to solve $-\nabla_H \cdot (\mathbf{K}_H \nabla_H p_H) = 0$, where the upscaled coefficient $\mathbf{K}_H$ is obtained from one of the known methods (see details in Sect. 4).

Upscaling of nonlinear models presents a challenge. In particular, consider a nonlinear PDE of the form

$$\nabla \cdot \mathcal{K}(\nabla p_h) = 0,$$

where $\mathcal{K}(\xi_h) = \mathcal{K}(\theta_h; \xi_h)$ is a general nonlinear function of ξ parameterized by some parameters θ, both given at scale h. In general, there is no guarantee that the nonlinearity $\mathcal{K}^*$ in the upscaled model

$$\nabla \cdot \mathcal{K}^*(\nabla p_H) = 0,$$

is parameterized in the same way as $\mathcal{K}$ is in the original model, and even if so, that these parameters are equal to some upscaled θ_H. In other words, in general it is not true that one has $\mathcal{K}^*(\xi_H) = \mathcal{K}(\theta_H;\ \xi_H)$. Rather, to identify $\mathcal{K}^*$, one has to consider a collection of nonlinear upscaled maps; these follow from solutions to local cell problems posed at the scale h with

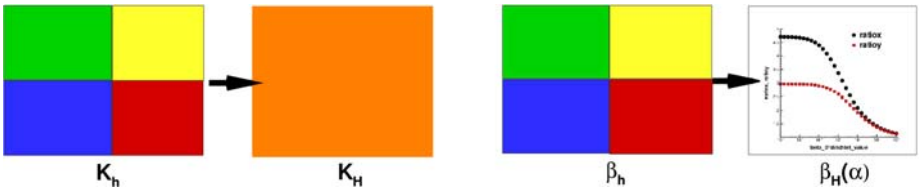

Fig. 1 Schematic difference between linear and nonlinear upscaling. *Left*: linear upscaling of $\mathbf{K}_h$ delivers a constant upscaled value $\mathbf{K}_H$. *Right*: nonlinear upscaling of β_h delivers a map $\beta_H(\alpha)$ where α represents a local boundary condition value

cells of size H but, in general, are not decoupled from the global equation (see Efendiev and Durlofsky 2002; Chen and Durlofsky 2006; Efendiev and Pankov 2004). Additional difficulties in using θ_H arise for systems even if they are linear (Peszyńska and Showalter 2007; see Fig. 1 for illustration).

In the problem of interest to this article, in the nonlinear PDE obtained from (1) and (3), we have $\mathcal{K}(\xi_h) = \mathcal{K}(\mathbf{K}_h, \beta_h; \xi_h)$. In what follows we show that upscaling of $\mathcal{K}$ gives a satisfactory upscaled model with $\mathcal{K}^*(\xi_H) = \mathcal{K}(\mathbf{K}_H, \beta_H; \xi_H)$, where the upscaled coefficients $\mathbf{K}_H, \beta_H$ are computed numerically via solutions to cell problems. It turns out that β_H is, in general, not constant but varies mildly with the average flow rates. We focus primarily on pressure-based upscaling after Durlofsky (1991).

As a result, we obtain an efficient and accurate method of upscaling (1). We believe that the success of this nonlinear upscaling procedure is due to the fact that the inertia effects appear to suppress heterogeneity of $\mathbf{K}$ for large β, which of course helps in the process of upscaling. In addition, we show that in some cases it is reasonable to use a simpler upscaled model with $\mathcal{K}^*(\xi_H) \approx \mathcal{K}(\mathbf{K}_H, \beta_H^{\mathrm{g}}; \xi_H)$ where β_H^{g} does not require nonlinear upscaling.

Nonlinear upscaling methods with applications to porous media have been applied to multiphase flow problems. There, in addition to deriving $\mathbf{K}_H$, one considers upscaling of nonlinear multiphase flow properties such as saturation-dependent relative permeabilities and/or capillary pressure relationships. The use of *pseudo-functions* (Barker and Thibeau 1996; Chen et al. 2005) is considered an effective yet not always fully satisfactory approach. Difficulty in upscaling multiphase models is associated with large heterogeneity contrasts, with dependence of multiphase flow properties on rock-type, as well as with the nonlinear coupled nature of systems of PDEs that have to be solved. For ongoing research, see Chen et al. (2003) and Chen and Durlofsky (2006).

On the other hand, there has been considerable research devoted to analysis (Fabrie and Langlais 1992) and numerical approximation (Douglas et al. 1993; Park 2005) of non-Darcy flow in homogeneous porous media. To our knowledge, however, not much work has been done for non-Darcy flow in heterogeneous media or devoted to the effects the Forchheimer correction has on the flow in heterogeneous case. In non-Darcy case, the only considerations known to us are in Narayanaswamy et al. (1999) where a scalar case is considered and recent work in Frih et al. (2008) where a separate approach applicable to fractured media is considered. In this article, we take a first step toward upscaling of non-Darcy flow for flow driven by boundary conditions only. When $q \not\equiv 0$, for example, when wells are present, non-Darcy flow in homogeneous media was considered in Ewing et al. (1999a); upscaling around wells for Darcy or for multiphase flow has been considered in Zijl and Trykozko (2001) and Chen and Yue (2003). Upscaling of non-Darcy flow around wells is outside the present scope.

The plan of the article is as follows. In Sect. 2 we give details of the model (1); we also provide analytical bounds and examples which show the connection between $\mathbf{K}$, β, and $\mathbf{u}$,

and effects of inertia associated with β on heterogeneity. These results help to explain the success of our upscaling procedure to be developed. In Sect. 3 we define the numerical discretization, with technical details deferred to Appendix. In Sect. 4 we define our upscaling approach, and in Sect. 5 we present results of the upscaling method.

Throughout the article we assume the nondimensional form of (1)–(3) so that $\Omega, \mathbf{K}, \mathbf{u}$ are represented in computational experiments by simple nondimensional quantities. In the presentation, we also assume $d = 2$ and $\Omega \ni \mathbf{x} = (x_1, x_2)$ and $\mathbf{u} = (u_1, u_2)$, with natural simplifications or extensions used when $d = 1, 3$. Gravity effects are not included in this article explicitly but are easily accounted for in the numerical implementation.

Let $\mathbf{K} = \mathbf{K}(\mathbf{x}), \mathbf{x} \in \Omega$ be a symmetric, bounded, and positive definite uniformly in $\mathbf{x}$ conductivity coefficient. We assume $\mathbf{K}$ is diagonal: $\mathbf{K} = \mathrm{diag}(K_1, \ldots K_d)$, i.e., the principal axes of permeability variation are aligned with the coordinates $\mathbf{x}$. We note that some pressure-based upscaling methods deliver a nondiagonal $\mathbf{K}_H$ even if the original $\mathbf{K}_h$ is diagonal; however, restriction to diagonal $\mathbf{K}_h$ makes the current exposition manageable, and we drop the off-diagonal terms in $\mathbf{K}_H$, should they arise. Henceforth, we assume that each of components satisfies $K_m(\mathbf{x}) \geq \kappa, m = 1, \ldots d$ for some $\kappa > 0$. In the isotropic case, we have $\mathbf{K} = K\mathbf{I}$.

2 Non-Darcy Model, Analytical Solutions, and Bounds for (1)

Various formulations of non-Darcy models exist and have been argued as valid in various regimes of flow. In general, it is recognized (Ergun 1952; Ergun and Orning 1949; Lake 1989; Bear 1972; Dullien 1979) that the non-Darcy flow effects are important in regions of high pressure gradients/high velocity, are due to inertia effects, and were originally connected to the onset of turbulence at porescale level. Specifically, for $1 < Re < 100$ the Darcy equation (2) should be replaced by its extended form including additional terms polynomial in velocity modeling inertia.

In most early works, an extended model for the scalar case proposed first by Forchheimer (1901) was used and validated in the laboratory

$$K^{-1}u + \beta|u|u = -\frac{\mathrm{d}p}{\mathrm{d}x}. \tag{5}$$

However, there is no uniform agreement on how this equation should be extended to two or three dimensions, how to account for anisotropy, or for multiphase flow. Porescale explanations of non-Darcy phenomena via averaging Navier–Stokes or Oseen flows (Ruth and Ma 1992; Bennethum and Giorgi 1997; Chen 1998; Dullien 1979; Marusić-Paloka and Mikelić 2000; Peszynska et al. 2009) suggest that the form (1) is appropriate, with a possible enhancement of the inertia term to include a full tensor. Our upscaling method does not depend on the particular form of (1), and the form of upscaled β_H suggests a tensor form more general than $\beta\mathbf{I}|\mathbf{u}|$ (see Sect. 5). However, at this point we do not know how successful our upscaling method is when applied to nonlinearities other than those in (1); this is subject of current and future research.

As concerns heterogeneity of porous media, it is one of its most distinctive properties, and it accounts for difficulties in analysis and numerical simulation not encountered in man-made materials science. Most of the heterogeneity in flow models is reflected by dependence of $\mathbf{K} = \mathbf{K}(\mathbf{x})$. As concerns β, the experiments in which the values of β were calculated for a given isotropic rock sample suggest that β may be correlated with various powers of K (Geertsma 1976). Also, β is high for carbonate rocks such as limestone and sandstone and

generally higher for vugular than for nonvugular rocks (Jones 1987). In general, it is reasonable to conclude that in heterogeneous nonisotropic porous media, $\beta = \beta(\mathbf{x})$ whenever $\mathbf{K} = \mathbf{K}(\mathbf{x})$.

In this article, we report, for simplicity, only on two variants of β, indexed by $\mathcal{B}$, which for isotropic $\mathbf{K} = K\mathbf{I}$ read

$$\beta = g_{\mathcal{B}}(\beta_0, K) = \begin{cases} \beta_0, & \mathcal{B} = 0 \\ \frac{\beta_0}{\sqrt{K}}, & \mathcal{B} = 1 \end{cases}. \tag{6}$$

More (Geertsma 1976; Jones 1987) can be easily incorporated. However, a special case of nonsmooth g, such as the one for fracture systems where inertia terms are neglected in the matrix, will not be considered here but is a topic of future work. See also Sect. 5.3.4 on our computational results regarding correlation. In general, β may actually vary with pressure and/or composition of fluids, and some formulations of (1) account for this (Douglas et al. 1993; Ewing et al. 1999a,b; Fabrie and Langlais 1992). For simplicity throughout this article, we consider a fixed single phase fluid and, hence, we lump the viscosity and density coefficients along with $\mathbf{K}$, β.

For nonisotropic diagonal $\mathbf{K}$, the correlations (6) should be considered componentwise; we find it therefore natural to allow for $\beta = (\beta_1, \beta_2)$ to be a vector. Nonisotropic β may also arise in the process of upscaling; a vector form of β does not introduce additional difficulties in a numerical model. With this, we rewrite (1) componentwise, with the coupling term between components given by $|\mathbf{u}| = \sqrt{\sum_{m=1}^{d} u_m^2}$,

$$(K_m^{-1} + \beta_m |\mathbf{u}|) u_m = -\frac{\partial p}{\partial x_m}, \quad m = 1, \ldots d. \tag{7}$$

A simplified version, in which the nonlinearity in velocity components is decoupled, is the one adapted in Ewing et al. (1999a), and it is a multidimensional analogue of (5),

$$(K_m^{-1} + \beta_m |u_m|) u_m = -\frac{\partial p}{\partial x_m}, \quad m = 1, \ldots d. \tag{8}$$

Since (7) is more general, it will be used as a basis for numerical models. Interestingly, in some numerical discretizations, a discrete version of (8) arises on its own from discretization of (7).

2.1 Analytical Solution and Bounds

It is not difficult to find an analytical solution u to (5). In the multidimensional case, it may no more be directly possible. Below, we derive bounds which are helpful in scalar and nonscalar cases.

2.1.1 Estimates for Scalar Case

Let $D = -\frac{\mathrm{d}p}{\mathrm{d}x}$. Rewrite (5) as

$$u = \mathcal{K}(D), \tag{9}$$

where $\mathcal{K}(D) = \mathcal{K}(K, \beta; D)$. Solving (5) gives the following

$$u = \mathcal{K}(K, \beta; D) = \begin{cases} 0, & D = 0, \\ KD, & \beta = 0, \\ \operatorname{sgn}(D) \frac{-K^{-1} + \sqrt{(K^{-1})^2 + 4\beta|D|}}{2\beta}, & \beta \neq 0, \quad D \neq 0, \end{cases} \tag{10}$$

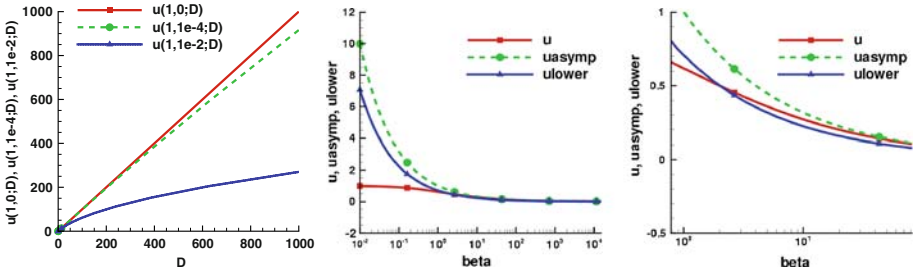

Fig. 2 Analytical solution $u = \mathcal{K}(K, \beta; D)$. *Left*: we show $\mathbf{u} = \mathcal{K}(1, \beta; D)$ for a fixed β in function of D. Note the deviation of non-Darcy velocity from linear Darcy velocity ($\beta = 0$). *Middle* and *right*: plot of $u = \mathcal{K}(1, \beta; 1)$ versus β and zoom of the figure. Both exact values and asymptotic bounds are shown

where $\mathrm{sgn}(D)$ denotes the sign of D. One can also write

$$u = \mathcal{K}(K, \beta; D) = \frac{2D}{K^{-1} + \sqrt{(K^{-1})^2 + 4\beta|D|}}, \tag{11}$$

from which it readily follows that $\mathcal{K}(K, \beta; D)$ is continuous in all arguments and parameters. Also, $\mathcal{K}$ is increasing in D but decreasing in β. See Fig. 2 for typical behavior of $u = \mathcal{K}(K, \beta; D)$. The calculation

$$\frac{\partial \mathcal{K}}{\partial D} = \frac{\mathrm{sgn}(D)}{\sqrt{(K^{-1})^2 + 4|D|\beta}} \tag{12}$$

with $\frac{\partial \mathcal{K}}{\partial D}|_{\beta=0} = K$ for Darcy flow, is useful in Jacobian (see Sects. 3 and 7.1).

2.1.2 *Bounds for u*

An expression equivalent to (11) is

$$u = \mathcal{K}(K, \beta; D) = \mathrm{sgn}(D)\left(-c + \sqrt{c^2 + \frac{|D|}{\beta}}\right), \quad c = \frac{K^{-1}}{2\beta}, \quad \beta \neq 0. \tag{13}$$

Clearly, since $-c + \sqrt{c^2 + \frac{|D|}{\beta}} \leq K D$, we have $\mathcal{K}(D) \leq K D$; i.e., the non-Darcy velocities do not exceed the Darcy velocities for the same pressure gradients. We recall that $\mathcal{K}^{-1}$ is sometimes called *a resistance parameter* which grows with increasing β or $|u|$ (Dullien 1979).

On the other hand, from $\frac{1}{\sqrt{2}}(r + q) \leq \sqrt{r^2 + q^2} \leq r + q$ for any $r, q \geq 0$, we see that, for $\beta \neq 0$

$$\mathcal{K}(K, \beta; D) \leq \sqrt{\frac{|D|}{\beta}} \tag{14}$$

$$\mathcal{K}(K, \beta; D) \geq \sqrt{\frac{|D|}{2\beta}} - \frac{K^{-1}}{2\beta}\left(1 - \frac{1}{\sqrt{2}}\right) \tag{15}$$

and that for large $\beta \geq \beta_{\text{crit}} = \frac{2}{|D|K^2}$, one actually has

$$\mathcal{K}(K, \beta; D) \geq \sqrt{\frac{|D|}{2\beta}}, \quad \beta \geq \beta_{\text{crit}}. \tag{16}$$

For $\beta \geq \beta_{\text{crit}}$, since $\mathcal{K}(K, \beta; D)$ decreases with β, we additionally have

$$\mathcal{K}(K, \beta; D) \leq \mathcal{K}(K, \beta_{\text{crit}}; D) = \frac{DK}{2}, \quad \beta \geq \beta_{\text{crit}}. \tag{17}$$

These bounds are useful in numerical calculations since they help to select a good initial guess for a local nonlinear solver.

More importantly, we obtain the asymptotics for large β which follows from (14) and (16),

$$u = \mathcal{K}(K, \beta; D) \approx \theta \sqrt{\frac{|D|}{\beta}}, \quad \theta \approx 1. \tag{18}$$

This approximation is quite revealing; it demonstrates that for really large inertia effects, the flux u is *essentially independent* of K. While u computed for realistic values of K, β, D found in porous media may not necessarily be in this asymptotic regime, (18) shows that the qualitative nature of u may be only mildly affected by heterogeneity of K, if large inertia effects are present. This is illustrated by numerical experiments shown in Fig. 3 where we see that with increasing β one obtains more smoothing of $\frac{\mathrm{d}p}{\mathrm{d}x}$.

For a given boundary condition, one can solve for p by integrating (10); we skip the calculation. This is not in general possible for the nonscalar case.

It is convenient to define the transmissibility (Peaceman 1977)

$$\mathcal{T}(K, \beta, \gamma, u) = \frac{1}{K^{-1} + \beta\sqrt{\gamma^2 + u^2}}, \tag{19}$$

and rewrite (5) in an implicit form as

$$u = \frac{D}{K^{-1} + \beta|u|} = \mathcal{T}(K, \beta, 0, u)D. \tag{20}$$

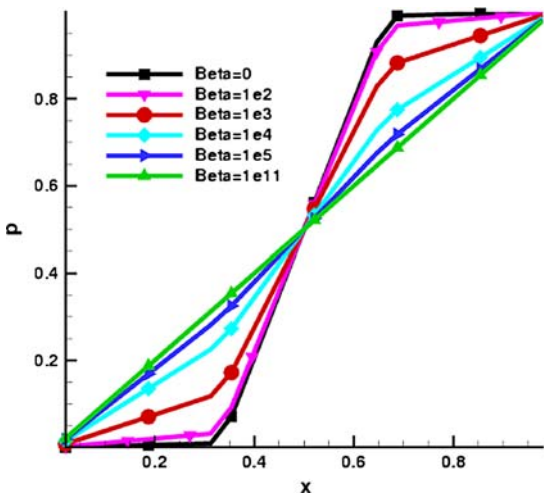

Fig. 3 Effects of inertia on heterogeneity. Shown is pressure solution for cross flow in a layered medium where K varies from 1 (left and right) to 10^{-4} in the middle part, for various values of β. Notice a sharp jump of pressure gradient for the case $\beta = 0$; the jump becomes smaller with larger β

2.1.3 Non-Scalar Case

Now we set $D_m = -\frac{\partial p}{\partial x_m}$, and use $\gamma^2 = \sum_{n\neq m}(u_n)^2$ which combines all components of velocity other than m, and we rewrite (7)

$$\left(K_m^{-1} + \beta_m \sqrt{\gamma^2 + (u_m)^2}\right) u_m = D_m. \tag{21}$$

We then have

$$u_m = \mathcal{T}\left(K_m, \beta_m, \sqrt{\sum_{n\neq 2} u_n^2}, u_m\right) D_m.$$

Note that $\mathcal{T}(K_m, \beta_m, \sqrt{\sum_{n\neq 2} u_n^2}, u_m) = \mathcal{T}(K_m, \beta_m, 0, |\mathbf{u}|)$; this simplifies the forthcoming numerical calculations discussed in Sect. 7.1.

Given $(u_n)_{n\neq m}$, i.e., γ, one can find u_m explicitly from (21) and/or derive estimates similar to those for the scalar case. In general of course, γ itself is unknown. However, given $D_m, m = 1, \ldots d$, one can solve (21) by fixed point or Newtonian iteration. Difficulties arise in numerical calculations because the discrete form of (21) involves a large stencil (see Sects. 3 and 7.2).

3 Numerical Discretization

Here, we formulate a discrete version of (3) and (1) as a cell-centered finite difference method (CCFD) in several variants depending on discretization of $|\mathbf{u}|$ in (7). These variants and discretization are motivated using mixed finite elements in Sect. 7.2; this development has a theoretical value in that the convergence results proved in Park (2005) for mixed FE methods apply to our discretization. Additionally, we obtain insight into why a particular discrete version of (7) is justified. From the point of view of upscaling, we show later that all the variants behave similarly; in other words, the success of upscaling is not tied to a particular variant of discretization.

Let the region Ω be decomposed into rectangular *elements* or *cells* Ω_{ij} on a Cartesian grid with natural notation of $\mathbf{x}_{ij} = (x_{1,ij}, x_{2,ij})$ denoting cell centers. The elements Ω_{ij} are of size $\triangle x_i \times \triangle y_j$. The edge $E_{i+1/2,j}$ between Ω_{ij} and $\Omega_{i+1,j}$ has a center at $(x_{1,i+1/2,j}, y_j)$, and so on. The distances between cell centers are denoted by $\triangle x_{i+1/2,j}$, etc. The parameter h is the maximum of either $\triangle x_i, \triangle y_j$. When coarse grid with parameter H is used, we index the cells using I, J.

The discrete pressures $p_h \equiv (p_{ij})_{i,j=1}$ are associated with cell centers. The normal components of velocities are associated with midpoints of cell edges; on the cell Ω_{ij} the velocity in direction x_1 is defined by its values $u_{1,i-1/2,j}$ on the left and $u_{1,i+1/2,j}$ on the right edges. The discrete velocities $\mathbf{u}_h$ can be then considered to be a tensor product of piecewise linear polynomials in x_1 direction and piecewise constant polynomials in the x_1 direction and opposite in the x_2 direction. The notation is standard (see Peaceman 1977; Russell and Wheeler 1983; Brezzi and Fortin 1991 for details).

Recall (Peaceman 1977; Russell and Wheeler 1983) the standard discrete counterpart of (3)

$$\nabla_h \cdot \mathbf{u}_h = 0, \tag{22}$$

and of (2), which we develop now. In the direction x_1 we have

$$u_{1,i+1/2,j} = K_{1,i+1/2,j} \frac{p_{i,j} - p_{i+1,j}}{\triangle x_{i+1/2,j}} = T_{1,i+1/2,j} \left(p_{i,j} - p_{i+1,j}\right), \tag{23}$$

where transmissibility $T_{1,i+1/2,j} = \frac{K_{1,i+1/2,j}}{\triangle x_{i+1/2,j}}$ is defined, and harmonic averaging of permabilities is used (Peaceman 1977):

$$K^{-1}_{1,i+1/2,j} = \frac{1}{2 \triangle x_{i+1/2,j}} \left(K^{-1}_{1,ij} \triangle x_i + K^{-1}_{1,i+1,j} \triangle x_{i+1}\right). \tag{24}$$

3.1 Discrete Non-Darcy Velocities

With notation as above, we can now state the following discrete counterpart of (1) or (7), with mixed finite element derivation deferred to Sect. 7.2:

$$\left(T^{-1}_{1,i+1,j} + \frac{1}{2}\left(\beta_{1,ij} \triangle x_i |\mathbf{u}_h|^+_{i,j} + \beta_{1,i+1,j} \triangle x_{i+1} |\mathbf{u}_h|^-_{i+1,j}\right)\right) u_{1,i+1/2,j} = p_{i,j} - p_{i+1,j}. \tag{25}$$

An analogous definition can be written immediately in direction x_2.

The crucial point is to define the terms $|\mathbf{u}_h|^+_{i,j}$ and $|\mathbf{u}_h|^-_{i+1,j}$. These have the meaning of magnitude of velocity on the cells i, j and $i + 1, j$, respectively, each relative to the edge $E_{i+1/2,j}$ on which the velocity component $u_{1,i+1/2,j}$ is being defined. They can be defined in several ways, which we denote below as variants $\mathcal{V} = 0, 1, 2, 3$.

Consider $|\mathbf{u}_h|^+_{i,j}$, with $|\mathbf{u}_h|^-_{i,j}$ defined analogously. The simplest way to define it ($\mathcal{V} = 0$) is to use the magnitude of normal component of $\mathbf{u}_h$ on the edge $E_{i+1/2,j}$, i.e., $|u_{1,i+1/2,j}|$, as was done in Ewing et al. (1999a).

Another way, $\mathcal{V} = 2$, is to use the magnitude of $\mathbf{u}_h$ itself on the edge $E_{i+1/2,j}$ which is defined using

$$(\bar{\mathbf{u}}_h)^+_{ij} = \left(u_{1,i+1/2,j}, \frac{u_{2,i,j+1/2} + u_{2,i,j-1/2}}{2}\right)$$
$$(\bar{\mathbf{u}}_h)^-_{ij} = \left(u_{1,i+1/2,j}, \frac{u_{2,i+1,j+1/2} + u_{2,i+1,j-1/2}}{2}\right),$$

or, with the quantity ($\mathcal{V} = 1$),

$$(\bar{\mathbf{u}}_h)_{ij} = \frac{(\bar{\mathbf{u}}_h)^+_{ij} + (\bar{\mathbf{u}}_h)^-_{ij}}{2}.$$

Finally, the most general way, called $\mathcal{V} = 3$, is to use the magnitude(s) of (interpolated) value(s) of

$$(\mathbf{u}_h)_{ij} = \left(\frac{u_{1,i+1/2,j} + u_{1,i-1/2,j}}{2}, \frac{u_{2,i,j+1/2} + u_{2,i,j-1/2}}{2}\right),$$
$$(\mathbf{u}_h)_{i+1,j} = \left(\frac{u_{1,i+1/2,j} + u_{1,i+3/2,j}}{2}, \frac{u_{2,i+1,j+1/2} + u_{2,i+1,j-1/2}}{2}\right),$$

in the middle of cells Ω_{ij} and $\Omega_{i+1,j}$, respectively.

Summarizing, we define

$$|\mathbf{u}_h|^+_{i,j} = \begin{cases} |u_{1,i+1/2,j}|, & \text{variant} = 0, \\ |(\bar{\mathbf{u}}_h)_{ij}|, & \text{variant} = 1, \\ |(\bar{\mathbf{u}}_h)^+_{ij}|, & \text{variant} = 2, \\ |(\mathbf{u}_h)_{ij}|, & \text{variant} = 3. \end{cases} \tag{26}$$

These four variants lead to somewhat different numerical solutions to (1)–(3).

Variant $\mathcal{V} = 0$ is a direct discretization of (8); it can also be seen as a simplification/approximation of variants $\mathcal{V} = 1, 2$. It uses the same five-point stencil as used for Darcy's law with diagonal $\mathbf{K}$ and allows for analytical componentwise resolution of local nonlinearities.

Variants $\mathcal{V} = 1, 2, 3$ are associated each with a different method of numerical integration in mixed FE applied to (7) (see Sect. 7.2). The difference between $\mathcal{V} = 1$ and $\mathcal{V} = 2$ is not larger than the one appearing in the use of numerical quadrature to derive (23) from (2) using mixed FE. Both variants couple the velocity $u_{1,i+1/2,j}$ to four other velocity degrees of freedom and are equivalent to each other up to higher order terms (see Sect. 7.2). With $\mathcal{V} = 1$, we have symmetry in that $|\mathbf{u}_h|^+_{i,j} = |\mathbf{u}_h|^-_{i+1,j}$, and one can get around the difficulty of an enlarged stencil when resolving local nonlinearities, by iteration lagging those components in $|(\bar{\mathbf{u}}_h)_{ij}|$ other than $u_{1,i+1/2,j}$. Variant $\mathcal{V} = 2$ is somewhat more complicated than $\mathcal{V} = 1$, because $|\mathbf{u}_h|^+_{i,j}$ is not identical to $|\mathbf{u}_h|^-_{i,j}$.

Variant $\mathcal{V} = 3$ is the most complex one, and, if applied in (25) alone, it couples velocity $u_{1,i+1/2,j}$ and pressures $p_{i,j}$, $p_{i+1,j}$ to six other velocity degrees of freedom appearing in its definition and thereby to 6 additional pressure values. The stencil in the resulting discrete system is increased from 5-point to 13-point in $d = 2$. In addition, resolution of local nonlinearity is not very successful by iteration lagging and impossible directly. While we performed numerical experiments with this variant, its complexity is not offering promise of being a successful model.

In view of the above, only $\mathcal{V} = 0, 1$ will be discussed further. In summary then, discretization of (7) or (8) takes the form

$$\left(T^{-1}_{1,i+1,j} + B_{1,i+1/2,j}|(\mathbf{u}_h)^{\mathcal{V}}_{i+1/2,j}|\right) u_{1,i+1/2,j} = p_{i,j} - p_{i+1,j}, \tag{27}$$

where we define $B_{1,i+1/2,j} = \frac{1}{2}\left(\beta_{1,ij} \triangle x_i + \beta_{1,i+1,j} \triangle x_{i+1}\right) = \triangle x_{i+1/2}\beta_{1,i+1/2,j}$, and where $|(\mathbf{u}_h)^{\mathcal{V}}_{i+1/2,j}|$ is computed according to (26).

It is convenient to cast (27) in a form similar to (23) and (20). Define the transmissibilities $\Upsilon^{\mathcal{V}}_{1,i+1/2,j}$ which, unlike $T_{1,i+1/2,j}$, depend nonlinearly on the solution,

$$\Upsilon^{\mathcal{V}}_{1,i+1/2,j} = \mathcal{T}\left(T_{1,i+1/2,j}, B_{1,i+1/2,j}, 0, |(\mathbf{u}_h)^{\mathcal{V}}_{i+1/2,j}|\right), \tag{28}$$

with a similar definition for $\Upsilon_{2,i,j+1/2}$. Now (27) reads, for every i, j

$$u_{1,i+1/2,j} = \Upsilon^{\mathcal{V}}_{1,i+1/2,j}(p_{i,j} - p_{i+1,j}), \tag{29}$$

$$u_{2,i,j+1/2} = \Upsilon^{\mathcal{V}}_{2,i,j+1/2}(p_{i,j} - p_{i,j+1}), \tag{30}$$

and in a vector form we can write symbolically, for $\mathbf{u}_h = \left((u_{1,i+1/2,j}, u_{2,i,j+1/2})\right)_{ij}$,

$$\mathbf{u}_h = \mathbf{T}^{\mathcal{V}}\left(\mathbf{K}_h, \beta_h, |\mathbf{u}_h|, \mathbf{u}_h\right) \nabla_h p_h = \mathbf{T}^{\mathcal{V}}_h \nabla_h p_h. \tag{31}$$

Note finally that if $\beta \equiv 0$ we have $\mathbf{T}^{\mathcal{V}}\left(\mathbf{K}_h, 0, |\mathbf{u}_h|, \mathbf{u}_h\right) \equiv -\mathbf{K}_h$. Also, recall that if $\mathcal{V} = 0$, the implicit relationships (29) and (30) can be resolved explicitly.

This formulation is used in the remainder of this article; see Sect. 7.2 for mixed FE derivation and Sect. 7.1 for details of nonlinear solver. Also, see Sect. 5 for discussion of the difference between variants $\mathcal{V} = 0, 1$. To complete this section, we comment on boundary conditions.

3.1.1 Boundary Conditions

In examples and upscaling procedures discussed in this article we consider one of the following types of boundary conditions, represented schematically in Fig. 4.

Let us be given Γ_D and Γ_N which denote the Dirichlet and Neumann no-flow parts of the boundary $\partial\Omega$, respectively. We impose

$$p|_{\Gamma_D} = p_D \tag{32}$$

$$\mathbf{K}\nabla p \cdot \nu|_{\Gamma_N} = 0. \tag{33}$$

Examples of Γ_D, Γ_N for a rectangular domain Ω denoted B1, B2, B3 and used in examples in Sect. 5 are shown in Fig. 4. Of course, other arrangements are possible.

In the numerical model, we apply Dirichlet boundary conditions using an algorithm shown in Peszyńska et al. (2002a,b). The no-flow Neumann conditions are natural for CCFD and are equivalent to setting transmissibilities on appropriate edges to 0 (Peaceman 1977).

For a rectangular domain Ω, instead of Dirichlet and Neumann conditions, one may choose to apply periodic boundary conditions (BP). Here, we discern between opposite sides of the rectangular domain, say Γ_- and Γ_+ and impose

$$p|_{\Gamma_+} = p|_{\Gamma_-} + \text{jump} \tag{34}$$

$$\mathbf{K}\nabla p \cdot \nu|_{\Gamma_+} = -\mathbf{K}\nabla p \cdot \nu|_{\Gamma_-}. \tag{35}$$

Here, the jump may be equal to 0, or not; usually, exactly one of the sides (left or right, top or bottom) will have a nonzero jump.

Implementation of periodic boundary conditions of the type (BP) shown in Fig. 4 is done by introducing an additional set of unknowns $p_{\partial\Omega}$. These unknowns play a dual role: first, they are used as the *known* values of "Dirichlet data." Second, their values on opposite sides of the domain are either matched or are subject to a prescribed jump. Finally, to close the system, the fluxes on opposite sides are matched. The system as such is underdetermined and one has to add an additional condition which fixes the average of p_h over Ω. In implementation, one can eliminate the additional unknowns $p_{\partial\Omega}$.

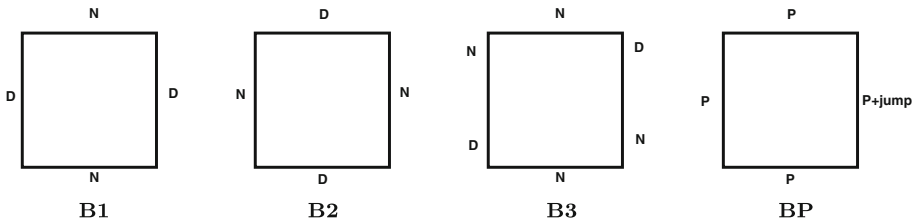

Fig. 4 Boundary conditions used in examples and upscaling procedures

4 Upscaling

This section provides answers to the core issues addressed in this article. Let us be given a scale h, identified as diameter of Ω_{ij}, on which the coefficients $\mathbf{K}_h, \beta_h$ are given, but at which it is practically impossible to solve the system (53). Assume there is a coarse scale $H \gg h$ at which such computations are possible. The main issue is to find the equations which describe the problem at scale H and to identify their coefficients. Our premise is that this is possible and that an upscaled version of (53)

$$\nabla_H \cdot \mathbf{T}_H^{\mathcal{V}} \nabla_H p_H = 0 \tag{36}$$

can be identified.

Alternatively, one can use a numerical method at scale H which incorporates the variation of $\mathbf{K}_h$ in its *definition*; this is done in subgrid upscaling or multiscale and variational approaches to finite element methods (see Arbogast 2003; Efendiev et al. 2000; Weinan et al. 2007; Efendiev and Pankov 2004; Efendiev et al. 2006 and related work). Yet another alternative is to use mortar upscaling (Peszyńska et al. 2002b).

Our approach in this article in using (36) is traditional, and we aim to derive $\mathbf{K}_H, \beta_H$ from $\mathbf{K}_h, \beta_h$. We briefly review what was done for Darcy flow and then proceed to non-Darcy case.

4.1 Upscaling $\mathbf{K}_h$ and Notation

For Darcy flow, it is standard to consider the upscaled linear system at scale H to be of the same form as the one at h, which is also linear. Various methods M of upscaling $(\mathbf{K})_h \mapsto (\mathbf{K})_H$ have been reviewed in Renarda and de Marsily (1997); these include arithmetic M = A or harmonic M $= \mathcal{H}$ averaging and give $(\mathbf{K})_H^{\mathrm{A}}$, $(\mathbf{K})_H^{\mathcal{H}}$, respectively. The *pressure-based* methods (Durlofsky 1991) which deliver $(\mathbf{K})_H^{\mathrm{D}}$,$(\mathbf{K})_H^{\mathrm{P}}$ and use Dirichlet and periodic boundary conditions, respectively, perform better than M $=$ A, $\mathcal{H}$ but are more computationally expensive. They are related to homogenization methods pursued in mathematical analysis (Bensoussan et al. 1978).

Here, we briefly recall the method proposed in Durlofsky (1991). Fix a grid cell Ω_{IJ} at scale H. By upscaling Darcy flow coefficients, we want to ensure that (23) holds on the grid H. Since (23) is linear, it is natural to ask that the fluxes on grid H which arise due to pressure gradients imposed on that grid, agree *on average* with fluxes on grid h, when these arise from the same global pressure gradients; this requirement preserves mass. With this approach, one finds $\mathbf{K}_H|_{\Omega_{IJ}}$ by inverse modeling as the appropriate coefficient of proportionality. The caveat is that one has to solve a cell problem on Ω_{IJ} subject to some global pressure gradients in order to compute that response. How these pressure gradients are imposed determines the D and P methods.

Consider first the local cell problem with Dirichlet boundary conditions of type B1 (see Fig. 4). We solve for $\tilde{p}_h, \tilde{u}_h$

$$-\nabla_h \cdot (\mathbf{K}_h \nabla_h \tilde{p}_h) = 0, \quad \mathbf{y} \in \Omega_{IJ} \tag{37}$$

$$\tilde{p}|_{\Gamma_{1,I-1/2,J}} = 0 \tag{38}$$

$$\tilde{p}|_{\Gamma_{1,I+1/2,J}} = D_{I,J} \tag{39}$$

$$(\mathbf{K}_h \nabla \tilde{p} \cdot \mathbf{n})|_{\Gamma_{2,I,J+1/2} \cup \Gamma_{2,I,J-1/2}} = 0. \tag{40}$$

Then, we compute the total flux $\tilde{u}_{1,I+1/2,J} = \int_{\Gamma_{1,I,J+1/2}} \tilde{u}_h \cdot \mathbf{n}$, and we find $K^{\mathrm{D}}_{1,I+1/2,J}$ by fitting it into the counterpart of (23)

$$\tilde{u}_{1,I+1/2,J} = K^{\mathrm{D}}_{1,I,J} \frac{D_{I,J}}{\triangle x_{I,J}}. \tag{41}$$

Next, we solve an analogous cell problem with boundary conditions B2 to find $K^{\mathrm{D}}_{2,I,J}$. The two values $K^{\mathrm{D}}_{1,I,J}$, $K^{\mathrm{D}}_{2,I,J}$ form the diagonal upscaled tensor $\mathbf{K}^{\mathrm{D}}_{I,J}$. Repeating cell calculations on all cells I, J of the grid at scale H, we obtain the collection of diagonal conductivities $\mathbf{K}_H \equiv \left(\mathbf{K}^{\mathrm{D}}_{I,J}\right)_{IJ}$.

Instead of using Dirichlet boundary conditions B1, B2, one can solve (37)–(40) subject to periodic boundary conditions (34) and (35) (see BP in Fig. 4). The jump is now D_{IJ}. However, the coefficients $(\mathbf{K}_H)^{\mathrm{P}}_{IJ}$ that one gets from inverse matching of fluxes across all boundaries are, in general, not diagonal even if $\mathbf{K}_h$ is diagonal.

The global system $-\nabla_H \cdot (\mathbf{K}_H \nabla_H p_H) = 0$ solved for p_H on grid H with $(\mathbf{K})^{\mathrm{M}}_H$ for $\mathrm{M} = \mathrm{D,P}$, has reasonable accuracy of global flow patterns in the sense that they resemble closely those for grid h. In general, $\mathrm{M} = \mathrm{P}$ leads to better accuracy of global flow patterns than $\mathrm{M} = \mathrm{D}$ does, and both are more accurate than $\mathrm{M} = \mathrm{A}, \mathcal{H}$. See further discussion of metrics of upscaling accuracy in Sect. 5.

4.2 Upscaling Non-Darcy Flow with a Pressure-Based Method

For non-Darcy flow, the underlying problem at scale h is nonlinear and, therefore, it is not straightforward to see whether the problem at scale H has the same structure as the one at scale h, and even if so, how to obtain $\mathbf{K}_h \mapsto \mathbf{K}_H$, and $\beta_h \mapsto \beta_H$.

The following idea comes to mind. Let us be given $\mathbf{K}_h$, β_h and some scale $H \gg h$. Let $\mathrm{M} = \mathrm{D}$, hence, we focus for the moment on a pressure-based method using Dirichlet boundary conditions. Consider Ω_{IJ} and compute solutions to the cell problem on Ω_{IJ} similar to (37) first setting $\beta_h \equiv 0$ (Darcy case). Next, we compute the solution with β_h as was given originally. In each cell $\Omega_{I,J}$, the former gives us $\mathbf{K}^{\mathrm{D}}_{IJ}$ while the latter can be used to find a nonlinear transmissibility $\Upsilon^{\mathrm{D},\mathcal{V}}_{IJ}$. Then, find the upscaled β^{D}_{IJ} by fitting the nonlinear transmissibility, $\mathbf{K}^{\mathrm{D}}_{IJ}$, D_{IJ}, and the fluxes to the analogue of (20) (see details in Sect. 4.2.1).

This procedure appears quite straightforward. However, the transmissibilities in non-Darcy flow depend nonlinearly on the fluxes; hence, β^{D}_{IJ} depends on the boundary conditions D_{IJ} driving the flow. In other words, β_H is not in general constant, but rather a function of gradients of pressure. When used in the global model (36), β_H will be chosen depending on p_H, or $\mathbf{u}_H$.

Therefore, the proposed procedure is only useful as a method of upscaling if (i) β_H satisfies the same qualitative properties that β_h does and (ii) we are able to determine *how it changes* quantitatively with the boundary conditions. In particular, (i) β_H should be positive. As concerns (ii), since Darcy's law and its discrete counterparts are linear, the coefficient $\mathbf{K}^{\mathrm{D}}_{I,J}$ does not depend on $\alpha = D_{IJ}$. However, the fluxes do, and therefore, the transmissibilities $\Upsilon^{\mathrm{D},\mathcal{V}}_{IJ}$ and hence, β^{D}_{IJ} also are functions of α.

Beside qualitative guesses, we found it impossible to predict the character of the map $\beta_H(\alpha)$ analytically. It has to be computed numerically but is found to vary only mildly (see Sect. 5.2). In general, only simple smooth relationships appear useful in practice so that it is enough to determine $\beta_H(\alpha)$ on a small set $\alpha \in A$: the values for $\alpha \in \mathbb{R}$ can be found via appropriate interpolation or approximation.

4.2.1 Details of Upscaling $\beta_h \mapsto \beta_H$

Now, we supply details of the method. Fix I, J. Consider variant $\mathcal{V} = 0$ or $\mathcal{V} = 1$. Find $\mathbf{K}^{\mathrm{D}}_{IJ}$ by solving (37)–(40). Next, consider the following extension of (37)–(40) to non-Darcy flow

$$-\nabla_h \cdot \left(\mathbf{T}_h^{\mathcal{V}} \nabla_h \hat{p}_h\right) = 0, \quad \mathbf{y} \in \Omega_{IJ} \tag{42}$$

$$\hat{p}|_{\Gamma_{1,I-1/2,J}} = 0 \tag{43}$$

$$\hat{p}|_{\Gamma_{1,I+1/2,J}} = D_{I,J} \tag{44}$$

$$(\mathcal{T}(\nabla_h \hat{p}_h) \cdot \mathbf{n})|_{\Gamma_{2,I,J+1/2} \cup \Gamma_{2,I,J-1/2}} = 0. \tag{45}$$

This cell problem is solved with the numerical method and Newtonian iteration described in Sects. 3 and 7.1.

Once $\hat{p}_h, \hat{u}_h$ are known, compute the total flux $\hat{u}_{1,I+1/2,J} = \int_{\Gamma_{1,I,J+1/2}} \hat{u}_h \cdot \mathbf{n}$, and find the value $\Upsilon^{\mathrm{D}}_{1,I,J}$ from (20)

$$\hat{u}_{1,I+1/2,J} = \Upsilon^{\mathrm{D}}_{1,I,J} \frac{D_{I,J}}{\triangle x_{I,J}}. \tag{46}$$

Finally, compute $\beta^{\mathrm{D}}_{1,IJ}$ from (20)

$$\beta^{\mathrm{D}}_{1,IJ} = \frac{\left(\Upsilon^{\mathrm{D}}_{1,I,J}\right)^{-1} - (K^{\mathrm{D}}_{1,IJ})^{-1}}{|\hat{u}_{1,I+1/2,J}|}. \tag{47}$$

Analogous calculations are done for $\beta_{2,IJ}$.

Collecting $\Upsilon^{\mathrm{D}}_{1,IJ}, \Upsilon^{\mathrm{D}}_{2,IJ}$ for all cells (I, J) we have Υ^{D}_H. By collecting $\beta^{\mathrm{D}}_{1,IJ}, \beta^{\mathrm{D}}_{2,IJ}$ computed componentwise, we finally obtain β^{D}_H.

Consider now M=P. It is straightforward to extend the above procedure to the case of periodic boundary conditions for cell problems; we have done this computationally. However, the process results in nondiagonal $\mathbf{K}^{\mathrm{P}}_H$, Υ^{P}_H and in more than two components of β^{P}_{IJ}. The resulting upscaled model for the full matrix β^{P}_H lacks a theoretical foundation, and we defer it to future investigation.

4.3 Other Methods of Upscaling β_h

Consider now $\mathrm{M} = \mathrm{A}, \mathcal{H}$ and simple averaging procedures which yield $K^{\mathrm{A}}_H, K^{\mathcal{H}}_H$.

Consider some divergence-free velocity field ψ_h on Ω_{ij} chosen ad hoc, i.e., without the pressure-solve of (42)–(45). For example, consider ψ_h arising as a gradient of linear pressure field satisfying (43)–(44), that is, a uniform velocity field. Note that since ψ_h is constant, trivially $\nabla_h \cdot \psi_h = 0$. Another possibility is to use as ψ_h the Darcy velocities found in (41). In each case, ψ_h depends linearly on D_{IJ}. Now, one can calculate a fixed quantity $\Upsilon(\mathbf{K}_h, \beta_h, \psi_h)$ which is "like" a transmissibility but which is inconsistent with (20). Putting aside the concern of inconsistency, a simple average $\Upsilon^{\mathrm{M}}_{IJ}$ of $\Upsilon(\mathbf{K}_h, \beta_h, \psi_h)$ for $\mathrm{M} = \mathrm{A}, \mathcal{H}$ can be computed. Following a calculation similar to (47) one obtains β^{M}_H for $\mathrm{M} = \mathrm{A}, \mathcal{H}$. This method of upscaling is very inexpensive computationally and may offer advantages in some cases especially in layered media. For lack of space we do not present results.

5 Results

Here, we illustrate results of the upscaling methodology proposed in Sect. 4 and we verify its accuracy; this follows in Sects. 5.2 and 5.3. For the sake of exposition, we provide first an illustration of numerical methods and effects of heterogeneity for non-Darcy flow (Sect. 5.1).

5.1 Non-Darcy Flow Results

Consider a 2D region of flow with $\mathbf{K}_h$ as shown in Fig. 5 with permeability field (a) layered isotropic, (b) periodic (similar to a fracture system), and (c) small heterogeneous. For each $\mathbf{K}_h$, let β_h be given by (6) with $\mathcal{B} = 0, 1$, and β_0 as indicated in each case. Now, solve the problem (53) subject to boundary conditions of type B1, B2, or B3, as shown in Fig. 4, with unit Dirichlet data. In the numerical model, we consider velocity variants $\mathcal{V} = 0, 1$ as in (26). Below follows a discussion of most interesting and at the same time simple enough cases.

As concerns the layered case (a), the results shown earlier in Sect. 2.1 in Fig. 2c are representative of cross-sections when $\mathbf{K}_h$ is layered and boundary conditions B1 are used. With large β_0, the profiles of pressure become more typical of those for a homogeneous medium. If boundary conditions B2 are used, the flow field is uniform; we skip the presentation of these results.

Results for the periodic field (b) are shown in Fig. 6. Here, we use boundary conditions B3 in order to make the flow patterns interesting enough. The same effect of smoothing effects of larger β_0 on pressure profiles is observed (Fig. 7).

Next, we show the effects of the choice of $\mathcal{B}$ and of $\mathcal{V}$; we focus on the heterogeneous case (c) and use $\beta_0 = 100$. See Fig. 8, where pressure profiles for different choices of $\mathcal{B}, \mathcal{V}$ are shown. It is evident that the solutions for different variants $\mathcal{V} = 0, 1$ do not differ much; this is also true for other values of β_0 (not shown). However, as expected, the solutions for different $\mathcal{B} = 0, 1$ differ substantially. This suggests that care must be taken in real simulations to determine an appropriate model (6) of β.

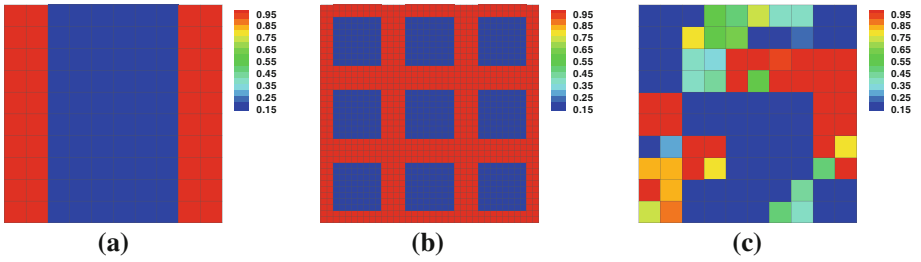

Fig. 5 Field $\mathbf{K}_h$ for three cases. (**a**) Layered. (**b**) Periodic (jump of a factor of 10). (**c**) Heterogeneous

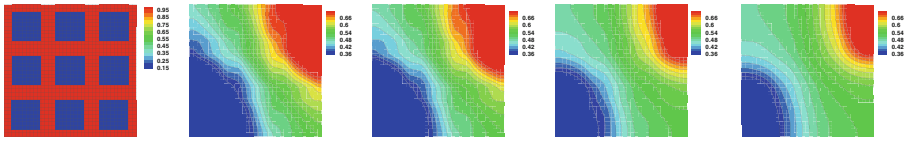

Fig. 6 Heterogeneity effects for non-Darcy flow, boundary condition B3, permeability field periodic, and $\mathcal{B} = 0, \mathcal{V} = 0$. *Far left*: reference field $\mathbf{K}_h$. *Left to right*: pressure profiles p_h for $\beta_0 = 0$ (Darcy), $\beta_0 = 1, 10^2, 10^3$, respectively

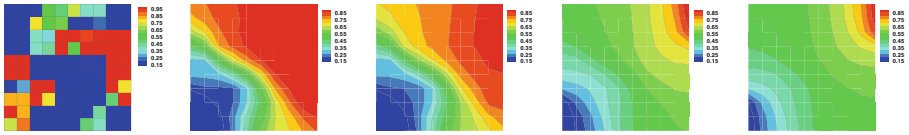

Fig. 7 Heterogeneity effects for non-Darcy flow, boundary condition B3, permeability field heterogeneous, and $\mathcal{B} = 0, \mathcal{V} = 0$. *Far left*: reference field $\mathbf{K}_h$. *Left to right*: pressure profiles p_h for $\beta_0 = 0$ (Darcy), $\beta_0 = 1, 10^2, 10^3$, respectively

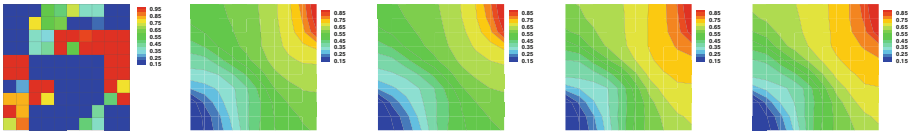

Fig. 8 Dependence of numerical solution on the choice of $\mathcal{B}, \mathcal{V}$. In all examples we use $\beta = 100$

5.2 Results of Upscaling

Now, we come to the central issue of this article on upscaling $\mathbf{K}_h, \beta_h$. Given $\mathbf{K}_h, \beta_h$ we want to (i) compute $\mathbf{K}_H, \beta_H$, (ii) use these to solve for p_H, and (iii) verify the accuracy of our upscaling procedure. Throughout this section we use $H = Nh$ with $N > 1$.

We restrict presentation to the method M = D using pressure-based solver with Dirichlet boundary conditions; as mentioned above, M = P leads to still open theoretical questions on the form of non-Darcy correction. Methods M = A, $\mathcal{H}$ are very simple but in general less accurate than M = D,P due to inconsistency and will not be discussed.

For logical verification of the upscaling methodology, we first set up a trivial problem with $\mathbf{K}_h \equiv \text{const} = \mathbf{K}_0$, with some given isotropic or anisotropic $\mathbf{K}_0$. Clearly, we obtain $\mathbf{K}_H = \mathbf{K}_0$ for any H. One can also expect that for any β_0 and $\beta_h = g_{\mathcal{B}}(\beta_0, \mathbf{K}_h)$, our upscaling procedure should deliver $\beta_H = g_{\mathcal{B}}(\beta_0, \mathbf{K}_H)$. This expectation is readily confirmed by numerical results for all cases $\mathcal{B} = 0, 1$, $\mathcal{V} = 0, 1$; detailed presentation is omitted.

Next, we consider nontrivial $\mathbf{K}_h$. We compute $\mathbf{K}_H$ (upscaled Darcy permeability) for $\mathbf{K}_h$, H as indicated in Fig. 9. We then let $\beta_h = g_{\mathcal{B}}(\beta_0, \mathbf{K}_h)$, consider $\mathcal{B} = 0, 1$ and $\mathcal{V} = 0, 1$ and use the upscaling procedure defined in Sect. 4 with Dirichlet boundary data $p_{\mathrm{D}} = \alpha$ which is allowed to vary and thus determine $\beta_H(\alpha)$. The collection of values α in practice need not be large.

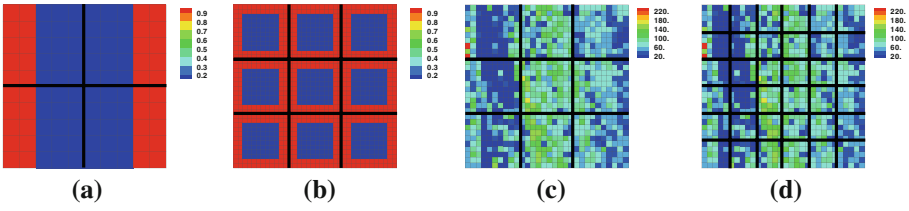

Fig. 9 Field $\mathbf{K}_h$ and grid H indicated by thick grid lines for three cases: (**a**) layered, (**b**) periodic, (**c**) large heterogeneous with 3×3 coarse grid, (**d**) large heterogeneous with 6×6 coarse grid

Of interest is variability of β_H on Dirichlet boundary data α, and its anisotropy, particularly when β_h itself is isotropic. In general, we find nonisotropic β_H even if β_h is isotropic, and that $\beta_H \neq g(\beta_0, \mathbf{K}_H)$.

In the case of constant β_h we find

$$\begin{aligned} \mathcal{B} = 0 : \beta_h &= g_0(\beta_0, K_h) \equiv \beta_0 \\ \beta_H(\alpha) &= \big(\beta_{H,1}(\alpha), \beta_{H,2}(\alpha)\big) = (\mathcal{R}_1(\alpha), \mathcal{R}_2(\alpha))\, \beta_0, \end{aligned} \tag{48}$$

where both ratios $\mathcal{R}_x, \mathcal{R}_y$, for a fixed β_0, are mildly varying functions of α.

In the correlated case we find, abusing notation as concerns diagonal components of $\mathbf{K}_h$ and $\mathbf{K}_H$,0

$$\begin{aligned} \mathcal{B} = 1 : \beta_h &= g_1(\beta_0, \mathbf{K}_h) = \frac{\beta_0}{\sqrt{K_h}}, \\ \beta_H(\alpha) &= \big(\beta_{H,1}(\alpha), \beta_{H,2}(\alpha)\big) = \frac{(\mathcal{R}_1(\alpha), \mathcal{R}_2(\alpha))\, \beta_0}{\sqrt{K_H}}. \end{aligned} \tag{49}$$

Remark 1 In summary, we find that

$$\beta_H(\alpha) = g_{\mathcal{B}}(\beta_0, \mathbf{K}_H)\, (\mathcal{R}_1(\alpha), \mathcal{R}_2(\alpha)), \tag{50}$$

i.e., β_H is constant or correlated to $\mathbf{K}_H$, up to a nonisotropic multiplicative correction dependent on α.

The usefulness of our upscaling procedure depends on the range and variability of $\mathcal{R}_i(\alpha)$, $i = 1, \ldots d$. In particular, in order for non-Darcy flow to retain its physical character reflected by monotonicity of the map $\mathcal{K}(K, \beta; D)$, we expect that each of the ratios must be positive; this is confirmed in our experiments. Results depend on $\mathbf{K}_h$, $\mathcal{B}$, and less significantly on $\mathcal{V}$ (see below). Finally, the variability of $\mathcal{R}_i(\alpha)$, $i = 1, \ldots d$ turns out to be small, and so our upscaling method in practice does not require tremendous computational effort: $\mathcal{R}_i(\alpha)$, $i = 1, \ldots d$ needs to be computed only for a few values of α.

5.2.1 Upscaled Map β_H for Layered Case

First, we discuss the results of the layered case, as they are quite illuminating (see Fig. 10). If $\mathcal{B} = 0$ and $\beta_h \equiv \beta_0$, it is at a first glance reasonable to expect that the upscaled $\beta_H = g_{\mathcal{B}}(\mathbf{K}_H) \equiv \beta_0$. However, this is in fact only true for the flow *across* the layers, where we see that $\mathcal{R}_1(\alpha) \equiv 1$. We hypothesize that this is due to harmonic weighting of transmissibilities which is in perfect agreement with arithmetic averaging of β_h and a constant unidirectional flux. On the other hand, the $\mathcal{R}_2(\alpha)$ is not constant and it is decreasing with α. In summary, in this case we obtain

$$\beta_H(\alpha) = (1, \mathcal{R}_2(\alpha))\beta_0. \tag{51}$$

However, we find that while β_H does indeed vary with both α and β_0, the ratios $\mathcal{R}_i$ remain mildly varying as functions of the product of $\beta_0\alpha$. Qualitatively, this is not surprising given the analytical solution derived in Sect. 2.1 (see also Fig. 2). From computational point of view, this property makes our upscaling method effective because results obtained for a fixed β_0 and several values of α can be reused for another set of values of β_0 and α.

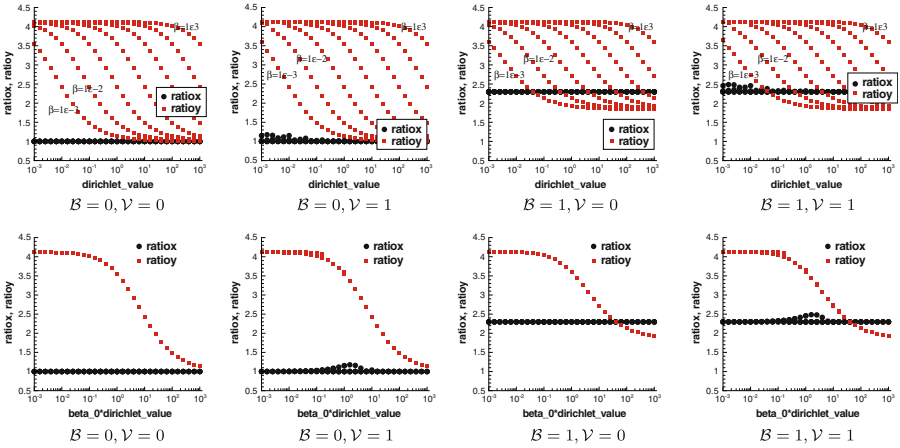

Fig. 10 Upscaled map $\beta_H(\alpha)$ for the layered case. Each figure shows $\mathcal{R}_1(\alpha)$, $\mathcal{R}_2(\alpha)$ called 'ratiox,ratioy', respectively, for various values of β_0. *Top*: dependence of $\mathcal{R}_i(\alpha)$. *Bottom* shows $\mathcal{R}_i$ as a function of the product $\alpha\beta_0$

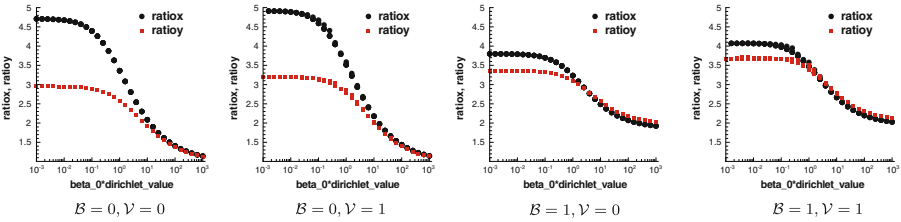

Fig. 11 Upscaled map $\beta_H(\alpha)$ for heterogeneous case when $\beta_h = g_{\mathcal{B}}(\beta_0, \mathbf{K}_h)$. Each figure shows $(\mathcal{R}_1, \mathcal{R}_2)$ denoted by ratiox, ratioy, respectively, as a function of the product $\alpha\beta_0$

5.2.2 Upscaled Map β_H for Heterogeneous Case

Observations similar to the layered case can be made for the periodic and heterogeneous cases, where $\mathbf{K}_h$ is as in Fig. 9b and c. Of these two, the heterogeneous case is more interesting; see results shown in Fig. 11. (We show only $(\beta_H)_{11}(\alpha)$.)

The main observation with respect to the layered case is that both $\mathcal{R}_i, i = 1, 2$ vary with α and β_0. This obviously results from nonuniform flow in both $x_i, i = 1, \ldots d$ directions.

5.3 Comparison of Fine and Coarse Grid Solutions

Now, we discuss the accuracy of upscaling non-Darcy flow by comparing results on coarse grid H to those on the original fine grid h.

In various articles devoted to upscaling, authors use different metrics to compare fine grid and coarse grid solutions; some compare p_h and p_H pointwise, some only show profiles of pressures and/or discuss agreement of velocity and streamline patterns between the two grids. In other articles, when wells are included, the well rates are compared. On the other hand, it was pointed out that minimizing a particular norm of $p_h - p_H$ may be associated with a particular upscaling method (see Holden and Nielsen 2000; Zijl and Trykozko 2002). In general, conclusions of comparisons depend on the metric that was chosen and on the

global boundary conditions and/or flow patterns. Finally, one should consider both accuracy and efficiency of an upscaling method.

In this article, we compare boundary fluxes across outflow parts of $\partial\Omega$

$$f = \int_{\Gamma_{\text{outflow}}} \mathbf{K}\nabla p \cdot \nu,$$

and we also consider the following.

Remark 2 In any comparison, one has to keep in mind the fact that, due to numerical error arising from discretization on grid h or H, the difference between solutions on grid h and H, regardless of the metrics, will likely be nonzero *even for homogeneous uniform* $\mathbf{K}_h$. (This does not apply directly to mortar or subgrid upscaling; see Peszyńska et al. 2002b; Peszyńska 2005; Arbogast 2003.) To alleviate the effect of discretization error on upscaling error, one can compare the solution p_h on grid h obtained using $\mathbf{K}_h, \beta_h$, to that $p_{H\mapsto h}$ computed on the same grid h but with data $\mathbf{K}_{H\mapsto h}, \beta_{H\mapsto h}$. Here by $\mathbf{K}_{H\mapsto h}, \beta_{H\mapsto h}$, we mean $\mathbf{K}_H, \beta_H$ which were *downscaled* to the original grid h, for example by simple injection. We found this method of comparison very useful, but it requires computation of a solution $p_{H\mapsto h}$ on grid h which is expensive and does not relate directly to p_H. We emphasize that this idea is suggested only for theoretical purposes to compare various upscaling methods M; in a practical upscaling simulation it would not be employed. See Table 1 for comparison of four upscaling methods $M = A, D, P, \mathcal{H}$ for Darcy case for all three types of boundary conditions B1, B2, and B3, for heterogeneous $\mathbf{K}_h$.

Now, we discuss results for non-Darcy upscaling; we test the accuracy of nonlinear upscaling relative to the accuracy of upscaling the linear Darcy case. We consider various patterns of $\mathbf{K}_h$ and H, shown in Fig. 9. As before, β_h is given by (6). We consider three cases of global

Table 1 Comparison of $M = A, D, P, \mathcal{H}$ for Darcy flow for heterogeneous $\mathbf{K}_h$

BC	M	f_h	f_H	$f_{H\mapsto h}$	$\lvert\frac{f_h - f_H}{f_h}\rvert$	$\lvert\frac{f_h - f_{H\mapsto h}}{f_h}\rvert$
B1	A	32.57484362	55.03545873	55.09824639	0.68950799	0.69143548
	D	32.57484362	32.35069719	32.38584459	0.00688097	0.00580199
	P	32.57484362	32.41986422	32.45464733	0.00475764	0.00368985
	$\mathcal{H}$	32.57484362	26.14566346	26.17359339	0.19736642	0.19650901
B2	A	51.38471961	58.92646422	58.97261428	0.14677018	0.14766831
	D	51.38471961	51.34424224	51.38080698	0.00078773	0.00007614
	P	51.38471961	50.55448835	50.58589065	0.01615716	0.01554604
	$\mathcal{H}$	51.38471961	35.73207110	35.77021427	0.30461679	0.30387449
B3	A	17.85362214	20.76764487	26.32567940	0.16321745	0.47452876
	D	17.85362214	13.98183753	17.75764287	0.21686269	0.00537590
	P	17.85362214	13.85705590	17.63303101	0.22385184	0.01235554
	$\mathcal{H}$	17.85362214	10.29882863	12.91371346	0.42315186	0.27668944

Note that flux f_H for $M = A$ / $M = \mathcal{H}$ seems to always overpredict/underpredict f_h; this is consistent with Hashin–Shtrikman bounds (Jikov et al. 1994; Renarda and de Marsily 1997). Also, $M = D, P$ give significantly more accurate results than $M = A, \mathcal{H}$. Note that $M = P$ which in general more accurate than $M = D$ here may be less so due to the off-diagonal terms of $\mathbf{K}_H^{\mathrm{P}}$ which are dropped. Finally, for more complicated flow pattern associated with B3, the use of downscaled solution shows that the coefficients $\mathbf{K}_H$ and the numerical error are jointly contributing to (in)accuracy of upscaled solution

Table 2 Layered case upscaled to 2×2

BC	D	β_0	f_h	f_H	$\lvert\frac{f_h - f_H}{f_h}\rvert$	f_H^{g}	$\lvert\frac{f_h - f_H^{\mathrm{g}}}{f_h}\rvert$
B1	1	0	0.15625	0.156250	0	0.156250	0
B2	1	0	0.46	0.460000	1.2e-016	0.460000	1.2e-016
B1	1	0.01	0.156212	0.156212	1.4e-013	0.156212	1.4e-013
	1	1	0.152611	0.152611	2.9e-015	0.152611	2.9e-015
	1	100	0.072995	0.072995	1.9e-016	0.072995	1.9e-016
	100	1	7.29952	7.299524	2.4e-016	7.299524	2.4e-016
	0.01	1	0.001562	0.001562	1.4e-013	0.001562	1.4e-013

Column BC describes the boundary condition used

boundary conditions B1, B2, and B3 as in Fig. 4 so that the flow is from right to left, top to bottom, or crossflow from right to left, respectively. We use a prescribed global gradient of pressure D and fix $\mathcal{B}, \mathcal{V}$.

We first compute $\mathbf{K}_H$ and the map β_H for each case, as shown in Sect. 5.2. To verify that it is important to *calculate* the upscaled map β_H via (48) and (49) rather than to use the original value or correlation, we also set

$$\beta_H^{\mathrm{g}}(\alpha) = g(\beta_0; \mathbf{K}_H). \tag{52}$$

Then, we solve for p_h on grid h and for p_H and p_H^{g} on grid H and compute fluxes.

Remark 3 To compute p_H, one needs to use the upscaled map $\beta_H(\alpha)$, i.e., we have to select the particular α that is needed. The α can be found by iteration lagging in global Newton iteration described in Sect. 7.1. Since $\beta_H(\alpha)$ does not have large derivatives, such estimation does not introduce much additional error.

Results corresponding to permeability cases from Fig. 9 are summarized in Tables 2, 3, and 4, respectively. Additionally, pressure profiles are shown for selected examples. Discussion then follows. For the sake of brevity as before, we restrict ourselves to only most interesting cases and results. Recall also that non-Darcy case results are only considered for $M = D$ for reasons explained above. We do not show downscaled results for lack of space; they are qualitatively consistent with nondownscaled results.

5.3.1 Upscaling of Layered Case

In the layered case and B1 and B2, the agreement of f_h and f_H is perfect. This is expected: for B1, the upscaled value $\mathbf{K}_H$ agrees with harmonic average, and for B2 with arithmetic average of $\mathbf{K}_h$, and this is reflected in the values of f_h, f_H for Darcy case $\beta = 0$. For $\beta \neq 0$, we have that β_H is constant and so $p_H = p_H^{\mathrm{g}}$ and we see also very good agreement of f_h with both f_H, f_H^{g}. Other results for B1 and B2 reproduce the same behavior.

5.3.2 Upscaling Periodic Case

In the periodic case, if β_H is used, the upscaled fluxes f_H are as accurate as in the layered case for all cases with $\mathcal{B} = 0, 1$ and $\mathcal{V} = 0, 1$. However, the fluxes f_H^{g} are not in very good agreement with f_h (see Table 3).

Table 3 Results of non-Darcy upscaling for periodic case upscaled to 3×3 grid

D	β_0	f_h	f_H	$\lvert\frac{f_h - f_H}{f_h}\rvert$	f_H^{g}	$\lvert\frac{f_h - f_H^{\mathrm{g}}}{f_h}\rvert$
1	0	0.451148	0.451148	8.06e-007	0.451148	8.06e-007
$\mathcal{V} = 0, \mathcal{B} = 0$						
	0.01	0.44762	0.447621	7.77e-007	0.450233	0.00583
	0.1	0.420943	0.420943	5.70e-007	0.442321	0.050787
	1	0.312592	0.312592	5.31e-008	0.384463	0.22992
	10	0.174966	0.174966	5.43e-007	0.224258	0.28172
	100	0.079319	0.079319	8.33e-007	0.089529	0.12872
1	0	0.451148	0.451148	8.06e-007	0.451148	8.1e-07
0.01	1	0.004473	0.004476	1.46e-005	0.004502	0.00594
0.1	1	0.042045	0.042050	0.000116	0.044232	0.05200
1	1	0.311185	0.311187	6.23e-006	0.384463	0.23547
10	1	1.74129	1.741323	2.04e-005	2.242580	0.28788
100	1	7.92272	7.922750	4.41e-006	8.952939	0.13003
$\mathcal{V} = 0, \mathcal{B} = 1$						
1	0	0.451148	0.451148	8.06e-007	0.451148	8.06e-007
1	0.01	0.447594	0.447595	7.77e-007	0.449789	0.00490
1	1	0.310331	0.310331	6.72e-008	0.362759	0.16894
1	100	0.0671734	0.067173	9.04e-007	0.074849	0.11426
$\mathcal{V} = 1, \mathcal{B} = 0$						
1	0	0.451148	0.451148	8.06e-007	0.451148	8.06e-07
	0.01	0.447573	0.447561	2.55e-005	0.450233	0.00594
	0.1	0.420478	0.420481	7.89e-006	0.442321	0.05194
	1	0.311185	0.311187	6.24e-006	0.384463	0.23547
	10	0.174126	0.174132	3.35e-005	0.224257	0.28790
	100	0.0792157	0.079227	0.000149	0.089529	0.13019

Here, we show results for B1 only, since the case is symmetric

5.3.3 Upscaling Heterogeneous Case

We consider isotropic and anisotropic variants. In the latter case, $(K_2)_{ij} = 5(K_1)_{ij}$. Results are, respectively, in Tables 4, and 5. It can be seen from Table 4 that the use of β_H gives significantly better results than the use of β_H^{g}. In particular, when comparing the results for $\beta = 0$ to those for $\beta \neq 0$, we see that the fluxes f_H are, at least for B1 and B2, quite close to f_h. In the nonisotropic case, the results of non-Darcy upscaling appear in better agreement than those with Darcy case (Figs. 12, 13, 14)

5.3.4 Correlation between β_H and $\mathbf{K}_H$

Our last result answers a natural question, and let $\mathcal{B} = 0$ and $\beta_0 = 1$. Let us be given a fine grid heterogeneous $\mathbf{K}_h$ such as in Fig. 9c. After $\mathbf{K}_H$ and $\beta_H(\alpha)$ are computed, the questions is: for a fixed α, is there any correlation between $\beta_H(\alpha)$ and $\mathbf{K}_H$?

Table 4 Results for heterogeneous, isotropic case

BC	D	β_0	f_h	f_H	$\lvert\frac{f_h - f_H}{f_h}\rvert$	f_H^{g}	$\lvert\frac{f_h - f_H^{\mathrm{g}}}{f_h}\rvert$
B1	1	0	32.5748	32.350697	0.0068809674	32.350697	0.00688
B2	1	0	51.3847	51.344242	0.00078773182	51.344242	0.00078773182
B3	1	0	17.8536	13.981838	0.21686269	13.981838	0.21686269
$\mathcal{B} = 0$ upscaling to 3×3							
B1	1	0.01	8.30372	8.292560	0.0013440962	8.535338	0.02789
	1	1	0.98079	0.980768	2.26e-005	0.984167	0.0034434907
	1	100	0.0998039	0.099805	9.14e-006	0.099840	0.00036680035
B1	0.01	1	0.0830359	0.082925	0.0013346016	0.085353	0.027909566
	1	1	0.98079	0.980768	2.26e-005	0.984167	0.0034434907
	100	1	9.98054	9.980541	8.34e-009	9.984043	0.0003509255
$\mathcal{B} = 1$ upscaling to 3×3							
B1	1	0.01	16.4825	16.581159	0.0059877337	16.736875	0.015435089
	1	10	0.771172	0.788014	0.021839215	0.758147	0.016889485
	1	1	2.36765	2.416472	0.020619331	2.335706	0.013492875
	1	100	0.246165	0.251634	0.022216664	0.241736	0.017991781
	10	1	7.71176	7.880148	0.0218355	7.581472	0.016894391
B2	1	0.01	8.46364	8.392461	0.0084098349	8.980445	0.061061964
	1	1	0.981007	0.980862	0.00014691914	0.989225	0.0083772249
	1	100	0.0998052	0.099805	4.8381498e-006	0.099892	0.00086514693
$\mathcal{B} = 0$ upscaling to 3×3							
B3	1	1	0.537621	0.443146	0.17572764	0.445521	0.17131009
	1	0.01	4.49917	3.685097	0.18093908	3.846547	0.14505487
	1	100	0.0548129	0.045192	0.17552435	0.045217	0.17507379
$\mathcal{B} = 1$ upscaling to 3×3							
B3	1	0.01	8.90008	7.152788	0.19632361	7.416759	0.16666418
	1	1	1.28143	1.047498	0.18255851	1.043956	0.18532221
	1	100	0.133437	0.109215	0.18152499	0.108140	0.18958172
$\mathcal{B} = 0$ upscaling to 6×6							
B1	1	0.01	8.30372	8.296412	0.00088023584	8.525850	0.0267505
	1	1	0.98079	0.980768	2.1964034e-005	0.984003	0.0032759738
	1	100	0.0998039	0.099804	2.4940728e-006	0.099838	0.00033819023
B2	1	0.01	8.46364	8.391858	0.0084810113	8.933469	0.055511652
	1	1	0.981007	0.980852	0.00015715651	0.988642	0.0077834603
	1	100	0.0998052	0.099805	1.6263878e-006	0.099885	0.00080476623

Upscaling to 3×3 and 6×6; only interesting cases shown. Throughout $\mathcal{V} = 0$

The answer is illustrated in Fig. 15, and it appears to suggest a mild correlation $\beta_H \approx c(\mathbf{K}_H)^s$ where $s < 0$ and $|s|$ is small, which is qualitatively independent of β_0 or α.

This *may* indicate why several authors report on *different* correlations between measured $\mathbf{K}$ and β; our calculations show that the computational correlations appear to depend on the scale at which they are measured.

Table 5 Heterogeneous case 30 × 30 with anisotropy ratio 5 upscaled to 3 × 3

BC	D	β_0	f_h	f_H	$\lvert\frac{f_h - f_H}{f_h}\rvert$	f_H^{g}	$\lvert\frac{f_h - f_H^{\mathrm{g}}}{f_h}\rvert$
B1	1	0	34.8733	33.689881	0.033933817	33.689881	0.033933817
B2	1	0	243.981	246.780723	0.011473481	246.780723	0.011473481
B3	1	0	24.5257	18.026847	0.26498012	18.026847	0.26498012
B1	1	0.01	8.32665	8.305207	0.0025747009	8.586365	0.031191334
	1	1	0.980837	0.980788	4.967377e-005	0.984753	0.0039928307
	1	100	0.0998053	0.099805	3.2948047e-007	0.099846	0.00041092264
B2	1	0.01	9.63034	9.625004	0.00055404447	9.776467	0.015173625
	1	1	0.996125	0.996118	6.3406493e-06	0.997739	0.0016202148
	1	100	0.0999578	0.099934	0.00023912392	0.099977	0.00019552109
B3	1	0.01	4.71649	3.821925	0.18966706	3.988913	0.15426174
	1	1	0.540639	0.444926	0.1770378	0.447171	0.17288422
	1	100	0.0548442	0.045206	0.1757355	0.045233	0.17524023

Throughout $\mathcal{B} = 0, \mathcal{V} = 0$

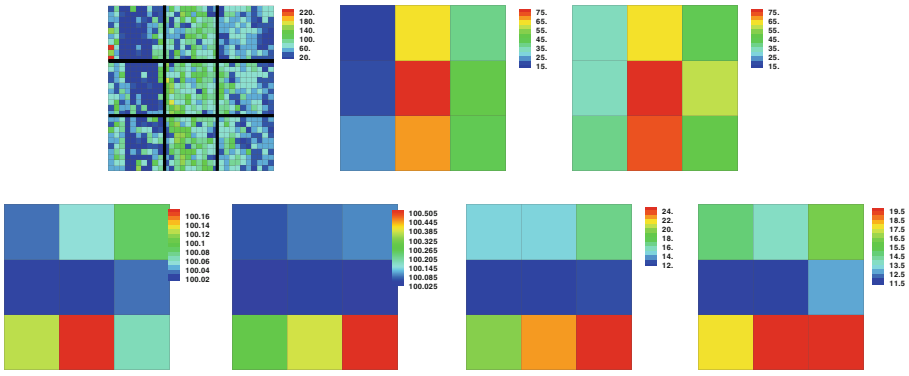

Fig. 12 Data for upscaling heterogeneous case to 3 × 3 grid. *First row*: original $\mathbf{K}_h$ (isotropic) and upscaled permeabilities $\mathbf{K}_H$ (nonisotropic). *Second row*: upscaled $\beta_{1,H}(1)$, $\beta_{2,H}(1)$ for $\beta_0 = 1\mathrm{e}2$ and $\mathcal{B} = 0$ (*left*) and $\mathcal{B} = 1$ (*right*)

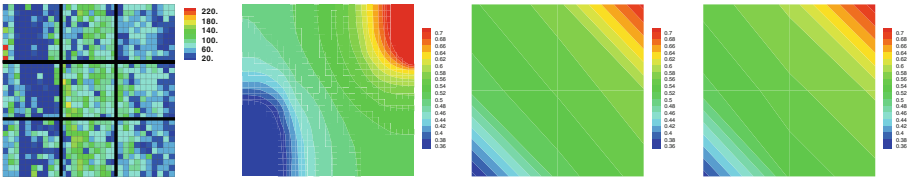

Fig. 13 Upscaling heterogeneous case to 3 × 3 grid with B3 boundary conditions: pressure contours for $\beta_0 = 100$, $\mathcal{B} = 0$. *Far left*: $\mathbf{K}_h$. *Left*: fine grid solution p_h, *middle*: p_H. *Right*: p_H^{g}

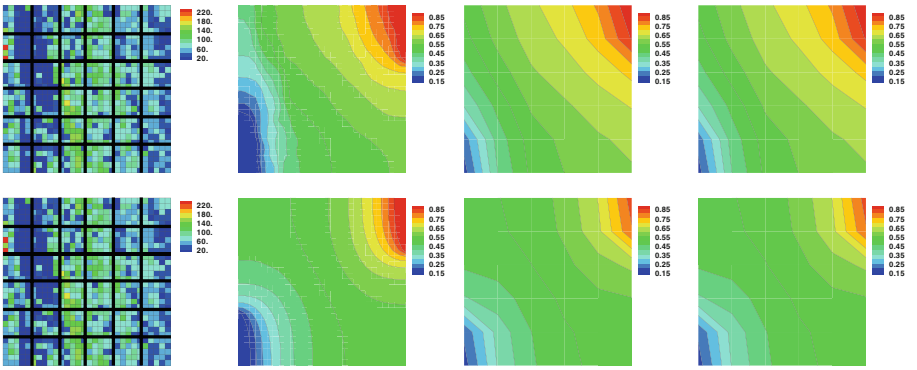

Fig. 14 Upscaling heterogeneous case to 6×6 grid with B3 boundary conditions: pressure contours for $\beta_0 = 0$ (*top*), and $\beta_0 = 1$. Throughout $\mathcal{B} = 0$. *Far left*: $\mathbf{K}_h$ and H. *Left*: fine grid solution p_h, *middle*: p_H. *Right*: p_H^{g}

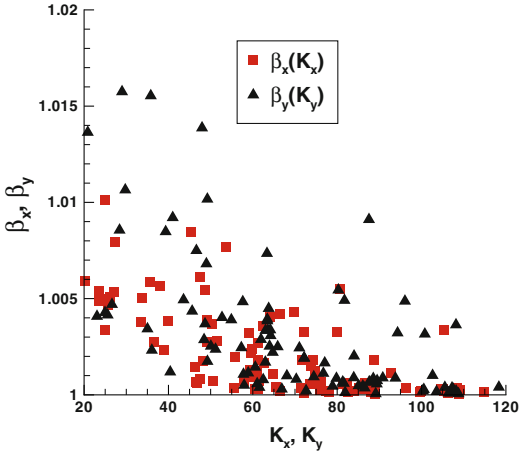

Fig. 15 Scatter-plot of $\beta_H(\alpha)$ versus $\mathbf{K}_H$ for $\alpha = 1$ for heterogeneous case

6 Conclusions

In this article, we have addressed the issue of upscaling non-Darcy flow driven by boundary conditions, where a simple quadratic model of velocity parametrized with a positive coefficient β and conductivity $\mathbf{K}$ extends the linear Darcy case. Given $\mathbf{K}_h$, β_h at fine scale h, the approach is to determine $\mathbf{K}_H$, β_H. Our method extends the one for Darcy case (Durlofsky 1991). The resulting upscaled coefficient β_H is a mildly varying map which supplies an anisotropic correction to the original coefficient from fine scale. We presented the numerical method, the upscaling procedure, and numerical results which demonstrate the accuracy of the method. Some simple variants of the procedure which may be less computationally cumbersome but are also less accurate have been also proposed. Values of β_H appear correlated to some function(s) of $\mathbf{K}_H$; this appears independent of the correlation at fine scale.

There remain open questions as concern an appropriate anisotropic model of non-Darcy correction, other non-Darcy models, fracture systems, as well as upscaling around wells. These are topics of future work.

Acknowledgements We would like to acknowledge the help of John Osborne (Oregon State University) with some upscaling computations. We thank Jill Reese for reference to Reese et al. (2006) where we found additional reference (Fourar et al. 2005) to the work on non-Darcy flow for layered media; we were not familiar with this work prior to submitting our article. Interestingly, our results concerning upscaled β_H for layered media appear consistent with those in Fourar et al. (2005). We would like to thank the anonymous referees whose remarks helped to improve the article. This study was partially supported by National Science Foundation grant 0511190 and Department of Energy grant 98089.

7 Appendix

7.1 Nonlinear Solver

Here, we discuss the solution of the nonlinear discrete system that arises from (22), some imposed boundary conditions, and the implicit relation (31). In summary, we solve for p_h the system

$$\nabla_h \cdot \mathbf{T}_h^{\mathcal{V}} \nabla p_h = 0. \tag{53}$$

This system of equations is nonlinear, and if $\mathcal{V} = 1$, it additionally requires a local internal iteration to resolve the local implicit relationships (29) and (30). The latter is not required for $\mathcal{V} = 0$.

Consider first $\mathcal{V} = 0$. One can compute explicitly $\mathbf{u}_h = \mathbf{T}^0(p_h)$ pointwise from (31), if only p_h is known. Since p_h is, of course, unknown, we have to solve (53) by iteration. As initial guess $p_h^{(0)}$ one can use the Darcy pressures which can be found by solving a linear counterpart of (53) setting $\beta = 0$. Or, for large β, additionally one may try the *method of continuity* in which one starts with $\beta = 0$ and then iterates, gradually increasing β to the desired magnitude, thereby obtaining a better initial guess.

It appears very natural to solve (53) using successive substitutions iterating on (31). Unfortunately, for small h and large heterogeneities, this simple iteration may have trouble converging and/or is very slow. The only reasonable alternative is to use Newton's method. We set it up as follows.

Given an initial guess $p_h^{(0)}$, iterate for $n = 0, 1, \ldots$ until convergence

$$\begin{aligned}
(*)\ \text{compute } \mathbf{u}_h^{(n)} &= \mathbf{T}^{\mathcal{V}}\left(\mathbf{K}_h, \beta_h, |\mathbf{u}_h^{(n)}|, \mathbf{u}_h^{(n)}\right) \nabla_h p_h^{(n)} \\
\text{compute residual } \mathbf{R}^{(n)} &= \nabla_h \cdot \mathbf{u}_h^{(n)} \\
\text{compute Jacobian } \mathbf{J}^{(n)} &= \frac{\partial}{\partial p_h} \mathbf{R}^{(n)} \\
\text{advance } p_h^{(n+1)} &= p_h^{(n)} - \left(\mathbf{J}^{(n)}\right)^{-1} \mathbf{R}^{(n)}
\end{aligned}$$

In this algorithm, the step $(*)$ can be executed pointwise analytically, if $\mathcal{V} = 0$. The residual calculations of $\mathbf{R}^{(n)}$ are quite simple as we only have to calculate the current $\nabla_h \cdot \mathbf{u}_h^{(n)}$. Jacobian calculations of $\mathbf{J}^{(n)}$ are done with the help of (12). Overall however, the method converges generally quite fast, even for large β.

Consider now $\mathcal{V} = 1$. Now the step $(*)$ cannot be executed exactly and, in order to resolve (21), we compute an iteration-lagged approximation $\tilde{\mathbf{u}}_h^{(n)}$ to $\mathbf{u}_h^{(n)}$ via

$$\tilde{\mathbf{u}}_h^{(n)} = \mathbf{T}^{\mathcal{V}}\left(\mathbf{K}_h, \beta_h, |\mathbf{u}_h^{(n-1)}|, \tilde{\mathbf{u}}_h^{(n)}\right) \nabla_h p_h^{(n)}.$$

This introduces a mild inconsistency in the residual and Jacobian calculations. However, the Newton iteration converges at least as fast as the one for $\mathcal{V} = 0$. If the iteration is run under strict convergence tolerance criteria, then one can assume that $\tilde{\mathbf{u}}_h^{(n)} \approx \mathbf{u}_h^{(n)}$. Note that due to a different formulation $p_h, \mathbf{u}_h$ obtained with $\mathcal{V} = 0, 1$ are (somewhat) different (see results shown in Sect. 5).

Our experience with performance of the Newton solver for variants $\mathcal{V} = 0, 1$, models $\mathcal{B} = 0, 1$ of β_h, and values of $\mathbf{K}_h$ can be summarized as follows. The solver needs more iterations in the case of strong anisotropy especially if β is correlated with $\mathbf{K}$. Next, one should formulate the stopping criteria very carefully: in terms of simple mass-balanced residual norms, the iteration appears not to be making much progress, while pressure and velocity values have not yet converged. As concerns velocity variants, variant $\mathcal{V} = 0$ requires more iterations to converge than $\mathcal{V} = 1$, especially for strong anisotropy ratio and large uncorrelated heterogeneities; this is likely caused by $\mathcal{V} = 1$ being capable of carrying more information. The opposite appears true for small correlation lengths, for example, for the periodic fissure problem (see Sect. 5) and is probably due to the inconsistency of residuals discussed above playing more substantial role in the absence of other difficulties.

7.2 Mixed FE Derivation of (25)

Here, we use mixed finite elements of type $RT_{[0]}$ on a rectangular grid to derive (25); we focus on details leading to (26). Such derivation was done for Darcy's flow in Russell and Wheeler (1983). The non-Darcy flow equations were discretized using mixed FE in Douglas et al. (1993) and Park (2005) but, to our knowledge, the use of quadrature and identification with CCFD discussed here has not been carried out. The importance of this derivation is that it extends the convergence results of mixed FE to CCFD formulation; on the other hand, it uncouples the saddle point formulation of mixed FE (Russell and Wheeler 1983). For notation see also Brezzi and Fortin (1991).

First consider the weak formulation of (1) and (4) complemented by no-flow boundary conditions (33) with $\Gamma_N \equiv \partial\Omega$. Let $(W, \mathbf{V}) = (L^2(\Omega), \{\mathbf{v} \in H(\mathrm{div}; \Omega) : \mathbf{v} \cdot \nu|_{\Gamma_N} = 0\})$. The weak solution $(p, \mathbf{u}) \in (W, \mathbf{V})$ satisfies the system obtained by multiplying (4) and (1) by test functions $w \in W$, $\mathbf{v} \in \mathbf{V}$ and integrating by parts over Ω

$$\int_\Omega \nabla \cdot \mathbf{u} w = \int_\Omega q w, \quad \forall w \in W, \tag{54}$$

$$\int_\Omega \mathbf{K}^{-1}\mathbf{u} \cdot \mathbf{v} + \int_\Omega \beta|\mathbf{u}|\mathbf{u} \cdot \mathbf{v} = \int_\Omega p \nabla \cdot \mathbf{v}, \quad \forall \mathbf{v} \in \mathbf{V} \tag{55}$$

The mixed FE solution $(p_h, \mathbf{u}_h) \in W_h \times \mathbf{V}_h$ where $W_h \subset W, \mathbf{V}_h \subset \mathbf{V}$. The functions in W_h are piecewise constant on each cell; a test function $\xi_{ij} \in W_h$ is a characteristic function of the cell $\Omega_{i,j}$ so that $p_h(x, y) = \sum_{ij} \xi_{ij}(x, y) p_{ij}$. Recall that the functions $\mathbf{v}_h \in \mathbf{V}_h$ from space $RT_{[0]}$ (Raviart and Thomas 1977) are piecewise linear in one coordinate direction and piecewise constant in the others and can be written symbolically as a tensor product $RT_{[0]} = P_{1,0} \times P_{0,1}$ (Brezzi and Fortin 1991; Russell and Wheeler 1983; Raviart and Thomas 1977). Here, $P_{q,r}(S)$ denotes a space of polynomials of degree q in x_1 and of degree r in x_2 which are variables over a subset $S \subset \mathbb{R}^d$. We have

$$\mathbf{u}_h(x, y)|_{\Omega_{ij}} = \big(\psi_{i-1/2,j}(x) u_{i-1/2,j} + \psi_{i+1/2,j}(x) u_{i+1/2,j}\ ,$$
$$\phi_{i,j-1/2}(y) v_{i,j-1/2} + \phi_{i,j+1/2}(y) v_{i,j+1/2}\big),$$

with the basis functions $\psi_{i\pm1/2,j}(x), \phi_{i,j\pm1/2}(y)$ in $P_{1,0}$ and $P_{0,1}$, respectively. Note that $\psi_{i+1/2,j}(x)$ is supported only on $\Omega_{ij} \cup \Omega_{i+1,j}$.

It is also useful to consider the value of $\mathbf{u}_h$ on the edge $E_{i+1/2,j,k} = \partial\Omega_{ij} \cap \partial\Omega_{i+1,j}$. By definition of $\mathbf{u}_h$, we are guaranteed the continuity of its normal component $(\mathbf{u}_h)_1$ but not of its tangential component $(\mathbf{u}_h)_2$ across that edge. The discrete solution $(p_h, \mathbf{u}_h)$ satisfies an equation analogous to (54) in which

$$\int_\Omega \nabla \cdot \mathbf{u}_h w_h = \int_\Omega q w_h, \quad \forall w_h \in W_h,$$

and using $w_h = \xi_{ij}$ one derives pointwise

$$u_{i+1/2,j} - u_{i-1/2,j} + u_{i,j+1/2} - u_{i,j-1/2} = q_{ij} \triangle x_i \triangle y_j, \tag{56}$$

which can be interpreted as (22) when $q \equiv 0$. The discrete analogue to momentum equation (55) is

$$\int_\Omega \mathbf{K}_h^{-1}\mathbf{u}_h \cdot \mathbf{v}_h + \int_\Omega \beta_h|\mathbf{u}_h|\mathbf{u}_h \cdot \mathbf{v}_h = \int_\Omega p_h \nabla \cdot \mathbf{v}_h, \quad \forall \mathbf{v}_h \in \mathbf{V}_h \tag{57}$$

forming a linear saddle-point system along with (22).

Now, as shown in Russell and Wheeler (1983) for Darcy flow, the integrals in (57) can be replaced by their numerical approximations, namely, a combination of trapezoidal and midpoint quadrature rules, at the expense of introducing a quadrature error of higher order than approximation order. In this way, the discrete velocity values are identified with those in CCFD formulation; the numerical integration approach entirely decouples the original saddle-point system and allows to solve a symmetric nonnegative-definite system in p_h unknown only. We notice that this is possible for diagonal $\mathbf{K}$.

We follow the same idea here for non-Darcy flow. Use the test function $\mathbf{v}_h = (\psi_{i+1/2,j}, \xi_{jk}) \in V_h$ and integrate over its support $\Omega_{ij} \cup \Omega_{i+1,j}$, with the trapezoidal rule applied to integration in x_1 direction and the midpoint rule applied in y_1 directions, which we denote by subscripts (TM).

The integration rules used below for products are all of second order accuracy with respect to the size of domain: trapezoidal $(\int_a^b f(t)g(t)\mathrm{d}t)_\mathrm{T} = (b-a)\frac{f(a)g(a)+f(b)g(b)}{2}$, the midpoint rule $(\int_a^b f(t)g(t)\mathrm{d}t)_\mathrm{M} = (b-a)f(\frac{a+b}{2})g(\frac{a+b}{2})$. Additionally, we define the product P rule as $(\int_a^b f(t)g(t)dt)_\mathrm{P} = (b-a)f(\frac{a+b}{2})\frac{g(a)+g(b)}{2}$. One can show using standard numerical analysis that the P rule has (at least) the same order of accuracy as the trapezoidal rule.

Using the (TM) rule for the first integral on left-hand side and integrating directly the right-hand side of (57), we obtain expressions as in Darcy's case, since $\mathbf{v}_h$ equals zero on both edges $E_{i-1/2,j}$, $E_{i+3/2,j}$

$$\begin{aligned}\left(\int_\Omega \mathbf{K}^{-1}\mathbf{u}_h \cdot \mathbf{v}_h\right)_\mathrm{TM} &= \left(\int_{\Omega_{ij}} K_{1,ij}^{-1}\mathbf{u}_h \cdot \mathbf{v}_h\right)_\mathrm{TM} + \left(\int_{\Omega_{i+1,j}} K_{1,i+1,j}^{-1}\mathbf{u}_h \cdot \mathbf{v}_h\right)_\mathrm{TM} \\ &= \triangle y_j T_{1,i+1/2,j}^{-1} u_{i+1/2,jk}, \\ \int_\Omega p_h \nabla \cdot \mathbf{v}_h &= \int_{\Omega_{ij}} p_{ij} \nabla \cdot \mathbf{v}_h + \int_{\Omega_{i+1,j}} p_{i+1,j} \nabla \cdot \mathbf{v}_h = \triangle y_j (p_{ij} - p_{i+1,j}).\end{aligned}$$

The new and most important element in the non-Darcy case is handling of the second term on the left side of (57). Using the (TM) quadrature rule over $\Omega_{ij} \cup \Omega_{i+1,j}$, we get

$$\left(\int_{\Omega} \beta|\mathbf{u}_h|\mathbf{u}_h \cdot \mathbf{v}_h\right)_{\mathrm{TM}} = \beta_{ij}\left(\int_{\Omega_{ij}} |\mathbf{u}_h|\mathbf{u}_h \cdot \mathbf{v}\right)_{\mathrm{TM}} + \beta_{i+1,j}\left(\int_{\Omega_{i+1,j}} |\mathbf{u}_h|\mathbf{u} \cdot \mathbf{v}\right)_{\mathrm{TM}} \tag{58}$$

Consider one of the integrals on the right side, which gives exactly

$$\left(\int_{\Omega_{ij}} |\mathbf{u}_h|\mathbf{u}_h \cdot \mathbf{v}\right)_{\mathrm{TM}} = \frac{\triangle x_i \,\triangle\, y_j}{2}|(\mathbf{u}_h)^+_{ij}|u_{1,i+1/2,j}, \tag{59}$$

and which is consistent with $\mathcal{V} = 2$ in (26) and the following expression

$$\begin{aligned}&\left(T^{-1}_{1,i+1/2,j} + \frac{1}{2}\left(\triangle x_i \beta_{1,ij}|\mathbf{u}_h|^+_{ij} + \triangle x_{i+1}\beta_{1,i+1,j}|\mathbf{u}_h|^-_{i+1,j}\right)\right)u_{1,i+1/2,j} \\ &= p_{i,j} - p_{i+1,j}.\end{aligned} \tag{60}$$

Since each $|\mathbf{u}_h|^+_{ij}$, $|\mathbf{u}_h|^-_{ij}$ depends on $u_{1,i+1/2,j}$ and on other velocity degrees of freedom, as mentioned before, the solution $u_{1,i+1/2,j}$ cannot be obtained analytically or even by local iteration.

This issue can be somewhat rectified by the use, instead of the discontinuous values $|\mathbf{u}_h|^+_{ij}$, $|\mathbf{u}_h|^-_{ij}$ in (60), of their average $|\bar{\mathbf{u}}_h|_{ij}$ as in $\mathcal{V} = 1$ leading to

$$\begin{aligned}&\left(T^{-1}_{1,i+1,j} + \frac{1}{2}(\triangle x_i \beta_{1,ij} + \triangle x_{i+1}\beta_{1,i+1,j})\left|\frac{(\mathbf{u}_h)^+_{ij} + (\mathbf{u}_h)^-_{i+1,j}}{2}\right|\right)u_{1,i+1/2,j} \\ &= p_{i,j} - p_{i+1,j}.\end{aligned} \tag{61}$$

This introduces an additional error which is however readily seen to be of order not exceeding that of numerical integration, via expansion, for any z, $\sqrt{1+z} = 1 + \frac{z}{2} - \frac{1}{8}z^2 + O(z^3)$. Further details will not be provided as they are not essential.

Now we discuss $\mathcal{V} = 3$. This arises if in (58) one uses the (PM) integration rule instead of (TM),

$$\left(\int_{\Omega_{ij}} |\mathbf{u}_h|\mathbf{u}_h \cdot \mathbf{v}\right)_{\mathrm{PM}} = \frac{\triangle x_i \,\triangle\, y_j}{2}|(\mathbf{u}_h)_{ij}|u_{1,i+1/2,j} \tag{62}$$

which provides the following alternative to (27),

$$\begin{aligned}&\left(T^{-1}_{1,i+1/2,j} + \frac{1}{2}\left(\triangle x_i \beta_{1,ij}|(\mathbf{u}_h)_{ij}| + \triangle x_{i+1}\beta_{1,i+1,j}|(\mathbf{u}_h)_{i+1,j}|\right)\right)u_{1,i+1/2,j} \\ &= p_{i,j} - p_{i+1,j}.\end{aligned}$$

Since this formulation leads to an excessively wide stencil, it is not pursued here.

Finally, we interpret $\mathcal{V} = 0$. It arises if instead of (7) one discretizes (8). Alternatively, $\mathcal{V} = 0$ can be seen as an approximation to $\mathcal{V} = 1$ in which the tangential components of velocity are ignored.

References

Arbogast, T.: An overview of subgrid upscaling for elliptic problems in mixed form. In: Current trends in scientific computing (Xi'an, 2002), Contemp. Math. **329**, 21–32 (2003)

Barker, J., Thibeau, S.: A criticial review of the use of pseudo relative permeabilities for upscaling. In: SPE 35491 (1996)

Bear, J.: Dynamics of Fluids in Porous Media. Dover, New York (1972)

Bennethum, L.S., Giorgi, T.: Generalized Forchheimer equation for two-phase flow based on hybrid mixture theory. Transp. Porous Media **26**(3), 261–275 (1997)

Bensoussan, A., Lions, J.L., Papanicolaou, G.: Asymptotic analysis for periodic structures. In: Studies in Mathematics and its Applications, vol. 5. North-Holland Publishing Co., Amsterdam (1978)

Brezzi, F., Fortin, M.: Mixed and hybrid finite element methods. In: Springer Series in Computational Mathematics, vol. 15. Springer-Verlag, New York (1991)

Chen, Z.: Expanded mixed finite element methods for linear second-order elliptic problems. I. RAIRO Modél. Math. Anal. Numér. **32**(4), 479–499 (1998)

Chen, Y., Durlofsky, L.J.: Adaptive local-global upscaling for general flow scenarios in heterogeneous formations. Transp. Porous Media **62**(2), 157–185 (2006)

Chen, Z., Yue, X.: Numerical homogenization of well singularities in the flow transport through heterogeneous porous media. Multiscale Model. Simul. **1**(2), 260–303 (electronic) (2003)

Chen, Y., Durlofsky, L.J., Gerritsen, M., Wen, X.H.: A coupled local global upscaling approach for simulating flow in highly heterogeneous formations. Adv. Water Resour. **26**, 1041–1060 (2003)

Chen, Z., Huan, G., Li, B.: A pseudo function approach in reservoir simulation. Int. J. Numer. Anal. Model. **2**(suppl.), 58–67 (2005)

Douglas Jr., J., Paes-Leme, P.J., Giorgi, T.: Generalized Forchheimer flow in porous media. In: Boundary Value Problems for Partial Differential Equations and Applications, RMA Research Notes in Applied Mathematics, vol. 29, 99–111, Masson, Paris (1993)

Dullien, F.: Porous Media. Academic Press, San Diego (1972)

Durlofsky, L.J.: Numerical calculation of equivalent grid block permeability tensors for heterogeneous porous media. Water Resour. Res. **27**(5), 699–708 (1991)

Durlofsky, L.: Upscaling of geological models for reservoir simulation: issues and approaches. Comput. Geosci. **6**, 569–571 (2002)

Efendiev, Y., Durlofsky, L.J.: Numerical modeling of subgrid heterogeneity in two phase flow simulations. Water Resour. Res. **38**(8), 3.1–3.11 (2002)

Efendiev, Y., Pankov, A.: Numerical homogenization and correctors for nonlinear elliptic equations. SIAM J. Appl. Math. **65**(1), 43–68 (electronic) (2004)

Efendiev, Y., Ginting, V., Hou, T., Ewing, R.: Accurate multiscale finite element methods for two-phase flow simulations. J. Comput. Phys. **220**(1), 155–174 (2006)

Efendiev, Y.R., Hou, T.Y., Wu, X.H.: Convergence of a nonconforming multiscale finite element method. SIAM J. Numer. Anal. **37**(3), 888–910 (electronic) (2000)

Ergun, S.: Fluid flow through packed columns. Chem. Eng. Prog. **48**, 89–94 (1952)

Ergun, S., Orning, A.: Fluid flow through randomly packed columns and fluidized beds. J. Ind. Eng. Chem. **41**, 1179–1184 (1949)

Ewing, R.E., Lazarov, R.D., Lyons, S.L., Papavassiliou, D.V., Pasciak, J., Qin, G.: Numerical well model for non-Darcy flow through isotropic porous media. Comput. Geosci. **3**(3–4), 185–204 (1999a)

Ewing, R.E., Wang, J., Weekes, S.L.: On the simulation of multicomponent gas flow in porous media. Appl. Numer. Math. **31**(4), 405–427 (1999b)

Fabrie, P., Langlais, M.: Mathematical analysis of miscible displacement in porous medium. SIAM J. Math. Anal. **23**(6), 1375–1392 (1992)

Frih, N., Roberts, J. E., Saada, A.: Modeling fractures as interfaces: a model for Forchheimer fractures. Comput. Geosci. **12**, 91–104 (2008)

Forchheimer, P.: Wasserbewegung durch Boden. Zeit. Ver. Deut. Ing. (45), 1781–1788 (1901)

Fourar, M., Lenormand, R., Karimi-Fard, M., Horne, R.: Inertia effects in high-rate flow through heterogeneous porous media. Transp. Porous Media **60**, 353–370 (2005). doi:10.1007/s11242-004-6800-6

Geertsma, J.: The effects of non-Darcy flow on the behavior of hydraulically fractured gas wells. J. Pet. Tech. **883**, 1169 (1976)

Holden, L., Nielsen, B.F.: Global upscaling of permeability in heterogeneous reservoirs; the output least squares (OLS) method. Transp. Porous Media **40**(2), 115–143 (2000)

Jikov, V.V., Kozlov, S.M., Oleinik, O.A.: Homogenization of differential operators and integral functionals. Springer-Verlag, Berlin (1994)

Jones, S.: Using the inertial coefficient beta to characterize heterogeneity in reservoir rock. In: SPE 16949, pp. 165–175 (1987)
Lake, L.W.: Enhanced oil recovery. Prentice Hall, Englewood Cliffs (1989)
Marusić-Paloka, E., Mikelić, A.: The derivation of a nonlinear filtration law including the inertia effects via homogenization. Nonlinear Anal. Ser. A Theory Methods **42**(1), 97–137 (2000)
Narayanaswamy, G., Sharma, M.M., Pope, G.: Effect of heterogeneity on the non-Darcy flow coefficient. SPE Reser. Eval. Eng. **2**(3), 296–302 (1999)
Park, E.J.: Mixed finite element methods for generalized Forchheimer flow in porous media. Numer. Methods Partial Differ. Equ. **21**(2), 213–228 (2005)
Peaceman, D.W.: Fundamentals of numerical reservoir simulation, 1st edn. Elsevier Scientfic Publishing Company, Amsterdam (1977)
Peszyńska, M.: Mortar adaptivity in mixed methods for flow in porous media. Int. J. Numer. Anal. Model **2**(3), 241–282 (2005)
Peszyńska, M., Showalter, R.E.: Multiscale elliptic-parabolic systems for flow and transport. Electron. J. Differ. Equ. (147), 30 pp. (electronic) (2007)
Peszyńska, M., Jenkins, E., Wheeler, M.F.: Boundary conditions for fully implicit two-phase flow model. In: Feng, X., Schulze, T.P. (eds.) Recent Advances in Numerical Methods for Partial Differential Equations and Applications. Contemporary Mathematics Series, vol. 306, pp. 85–106. American Mathematical Society, Providence (2002a)
Peszyńska, M., Wheeler, M.F., Yotov, I.: Mortar upscaling for multiphase flow in porous media. Comput. Geosci. **6**, 73–100 (2002b)
Peszynska, M., Trykozko, A., Augustson, K.: Computational modeling of inertia effects at porescale. In: Allen, G., Nabrzyski, J., Seidel, E., van Albada, D., Dongarra, J., and Sloot, P. (eds.) ICCS 2009 Proceedings, Springer Lecture Notes in Computer Science (2009, accepted)
Raviart R.A., Thomas J.M.: A mixed finite element method for 2nd order elliptic problems. In: Mathematical Aspects of the Finite Element Method, Lecture Notes in Mathematics, vol. 606, 292–315. Springer-Verlag, New York (1977)
Reese, J.P., Long, K.R., Kelley, C.T., Gray, W.G., Miller, C.T.: Simulating non-Darcy flow through porous media using sundance. In: Binning, P.J., Engesgaard, P.K., Dahle, H.K., Pinder, G.F., Gray, W.G. (eds.) Proceedings of the XVI International Conference on Computational Methods in Water Resources, Copenhagen. http://proceedings.cmwr-xvi.org (2006)
Renard, P., de Marsily, G.: Calculating effective permeability: a review. Adv. Water Resour. **20**, 253–278 (1997)
Russell T.F., Wheeler M.F. (1983) Finite element and finite difference methods for continuous flows in porous media. In: Ewing, R.E. (ed.) The Mathematics of Reservoir Simulation, pp. 35–106. SIAM, Philadelphia
Ruth, D., Ma, H.: On the derivation of the Forchheimer equation by means of the averaging theorem. Transp. Porous Media **7**(3), 255–264 (1992)
Weinan, E., Engquist, B., Li, X., Ren, W., Vanden-Eijnden, E.: Heterogeneous multiscale methods: a review. Commun. Comput. Phys. **2**(3), 367–450 (2007)
Zijl, W., Trykozko, A.: Numerical homogenization of the absolute permeability tensor around wells. SPE J., **5**, 399–408 (2001)
Zijl, W., Trykozko, A.: Numerical homogenization of two-phase flow in porous media. Comput. Geosci. **6**(1), 49–71 (2002)